Posted on 14 Nov 2023 — The copyright holder is the author/funder. All rights reserved. No reuse without permission. — https://doi.org/10.22541/essoar.170000392.22424750/v1 — This is a preprint and has not been peer-reviewed. Data may be preliminary.

Wavelet Analysis for Automatic Detection of Pi-2 Pulsations during Substorm Onset Along the 210$ˆ{\circ}$ Magnetic Meridian

stephen Owino Omondi[1], Akimasa Yoshikawa[2], Teiji Uozumi[3], Yuki Obana[4], Moe Hayashi[2], and Ayman Mohamed Mahrous[5]

[1]Egypt Japan University of Science and Technology
[2]Kyushu University
[3]Space Environment Research Center, Kyushu University
[4]Osaka Electro-Communication University
[5]Space Weather Monitoring Center, Helwan University, Faculty of Science

November 14, 2023

Abstract

Ground Pi-2 pulsations comprise superpositions of various modal components of shear and fast Alfven waves, field line resonance, and plasmaspheric resonances. These complex waveforms, hard to resolve with Fourier transforms are successfully characterized by wavelet techniques. Wavelet detection employs decomposition and reconstruction modes to characterize time-frequency components. Hence, suitable for the examination of the locality and complexity of natural signal patterns. The current study presents the automatic detection of Pi-2 pulsations using Daubechies and Morlet wavelet transforms. In the study, distinct Pi-2 events from CPMN stations along 210${ˆ\circ}$ magnetic meridian were detected. Global Pi-2 pulsations with harmonious H oscillations and discrete D bays in the sub-aurora zone suggest a common source with diverse tunneling paths. Scalograms of Pi-2 undulations of the frequency band of 6.7-22 mHz were observed despite different kinds of Pi-2s. Auroral Pi-2s were highly localized in local time with clear H and D bays, implying magnetospheric-ionospheric current couplings. Latitudinal and longitudinal Pi-2 propagations are exemplified by 180${ˆ\circ}$ phase-shift (polarization) in EWA and group delay in the mid-latitudes of the northern hemisphere. Overall, Pi-2 wave power from high to low latitudes declined with peak amplitudes of 15 nT to less than 1 nT, respectively. Finally, external influences from sea currents causing signal attenuation due to the station's proximity to the sea were also identified. To conclude, the accuracy and efficiency of wavelet analysis with no computation hassle render it a valuable tool for the study of space events in the magnetospheric community.

Posted on 14 Nov 2023 — The copyright holder is the author/funder. All rights reserved. No reuse without permission. — https://doi.org/10.22541/essoar.170000392.22424750/v1 — This is a preprint and has not been peer-reviewed. Data may be preliminary.

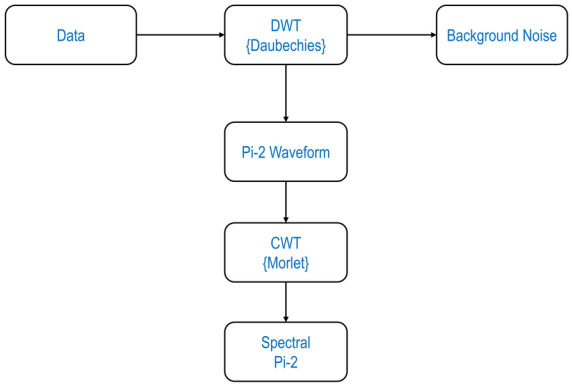

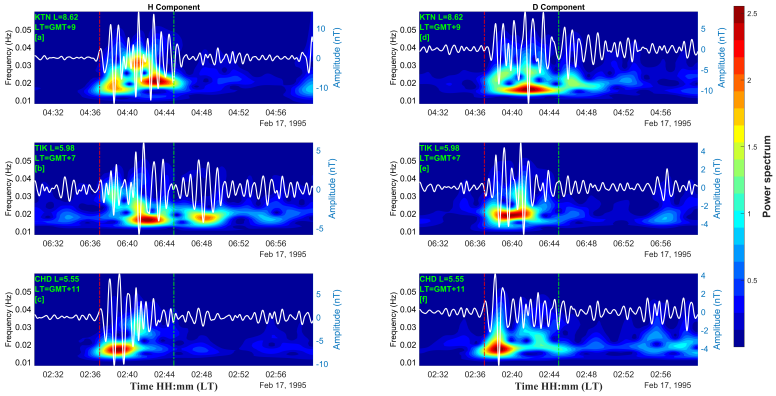

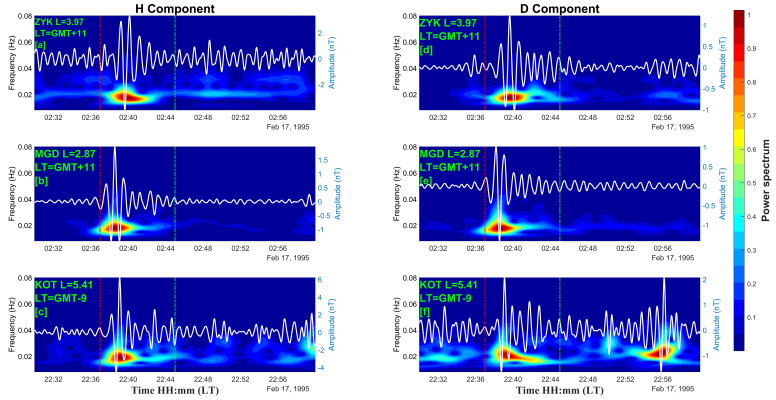

Posted on 14 Nov 2023 — The copyright holder is the author/funder. All rights reserved. No reuse without permission. — https://doi.org/10.22541/essoar.170000392.22424750/v1 — This is a preprint and has not been peer-reviewed. Data may be preliminary.

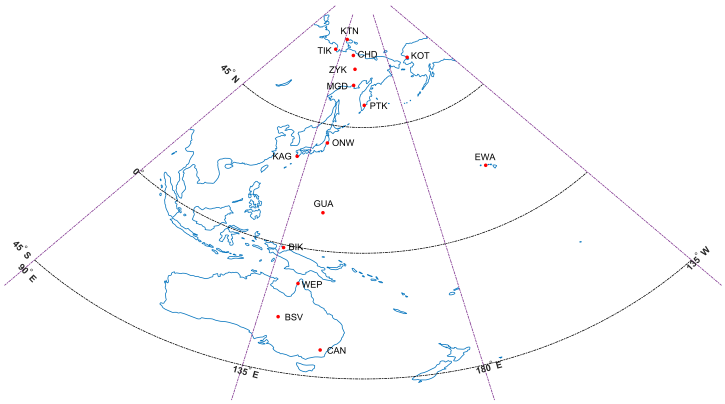

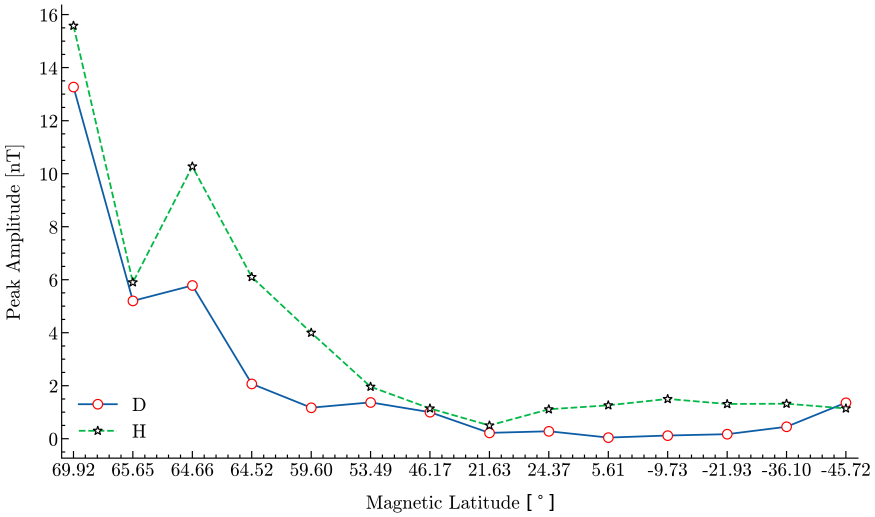

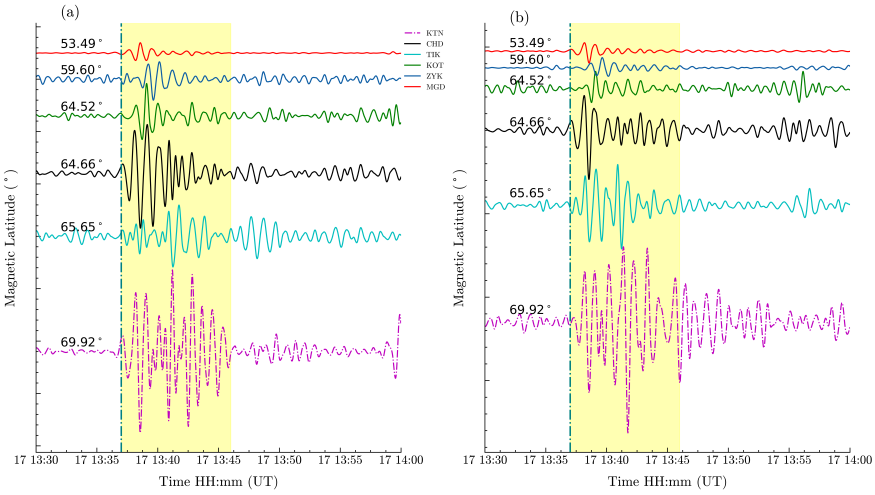

Posted on 14 Nov 2023 — The copyright holder is the author/funder. All rights reserved. No reuse without permission. — https://doi.org/10.22541/essoar.170000392.22424750/v1 — This is a preprint and has not been peer-reviewed. Data may be preliminary.

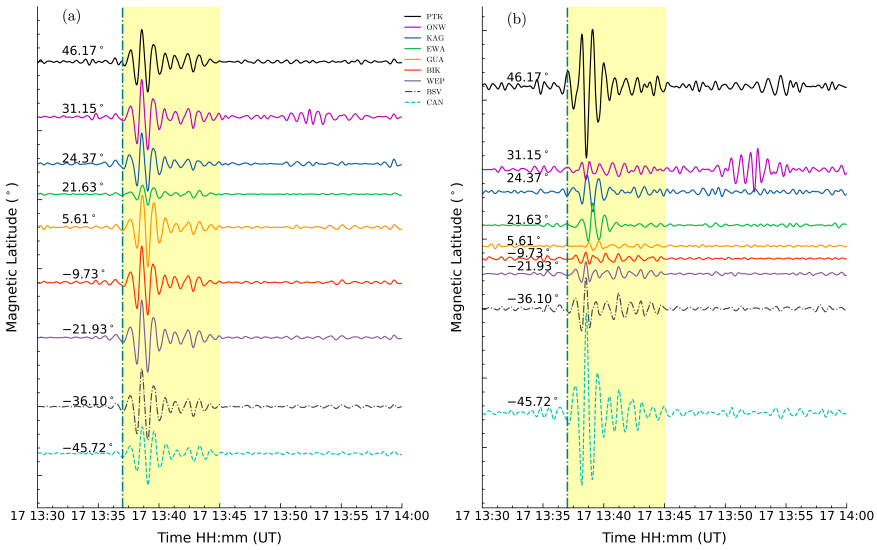

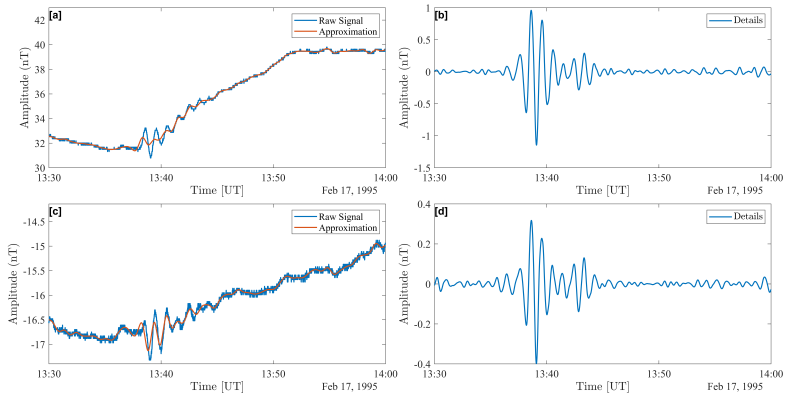

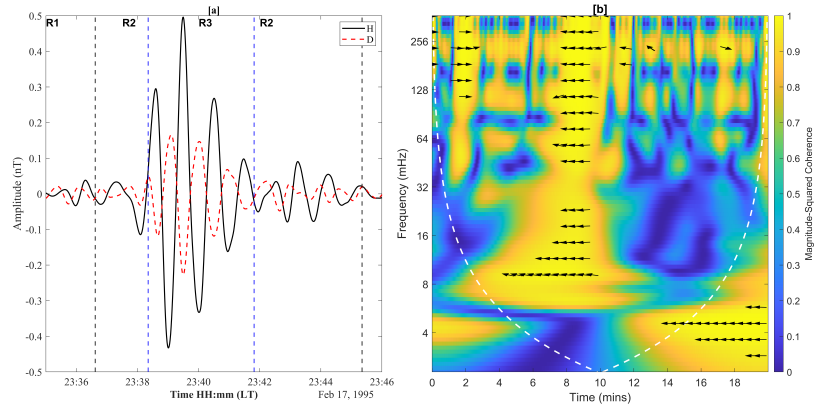

Posted on 14 Nov 2023 — The copyright holder is the author/funder. All rights reserved. No reuse without permission. — https://doi.org/10.22541/essoar.170000392.22424750/v1 — This is a preprint and has not been peer-reviewed. Data may be preliminary.

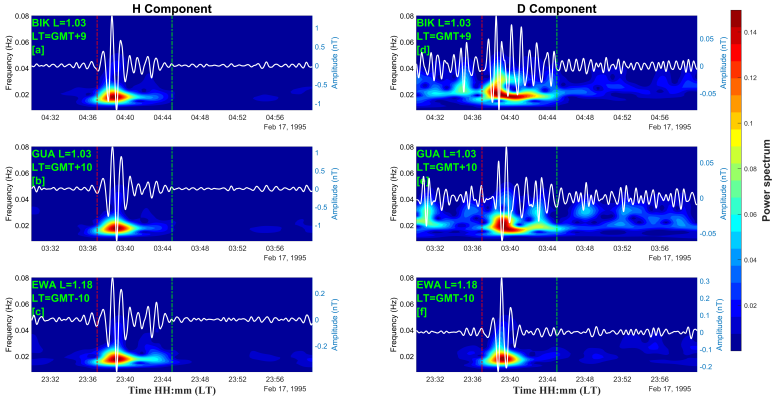

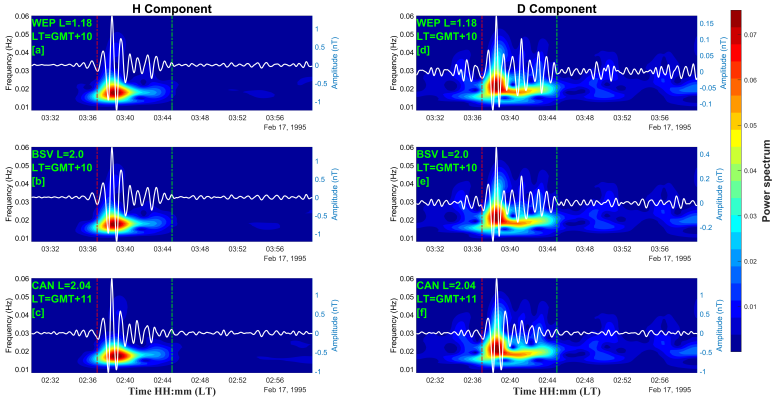

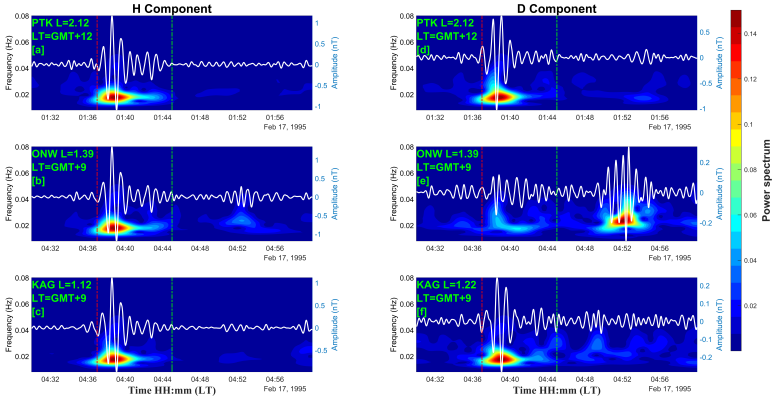

Wavelet Analysis for Automatic Detection of Pi-2 Pulsations during Substorm Onset Along the 210° Magnetic Meridian

Stephen Omondi[1,2], Akimasa Yoshikawa[2,3], T. Uozumi[2,3], Yuki Obana[2,3], Moe Hayashi [2,3], Ayman Mahrous[1,4]

[1]Department of Space Environment, Institute of Basic and Applied Sciences, Egypt-Japan University of Science and Technology (E-JUST), New Borg El-Arab City, Alexandria 21934, Egypt
[2]International Center for Space Weather Science and Education, Kyushu University, Fukuoka, Japan
[3]Department of Earth and Planetary Science, Kyushu University, Fukuoka, Japan
[4]Department of Physics, Faculty of Science, Helwan University, Helwan, Cairo, Egypt

Key Points:

- Wavelet automatic detection performed excellently well in Pi-2 detection from auroral to sub-auroral zone.
- Manifestations of latitudinal and longitudinal Pi-2 undulations illustrated by the ellipticities and group delays.
- Influence of dominance of external effect such as sea currents were uncovered resulting in Pi-2s heavily attenuated.

Corresponding author: Stephen Omondi, stephen.owino.omondi@outlook.com

Abstract

Ground Pi-2 pulsations comprise superpositions of various modal components of shear and fast Alfven waves, field line resonance, and plasmaspheric resonances. These complex waveforms, hard to resolve with Fourier transforms are successfully characterized by wavelet techniques. Wavelet detection employs decomposition and reconstruction modes to characterize time-frequency components. Hence, suitable for the examination of the locality and complexity of natural signal patterns. The current study presents the automatic detection of Pi-2 pulsations using Daubechies and Morlet wavelet transforms. In the study, distinct Pi-2 events from CPMN stations along 210° magnetic meridian were detected. Global Pi-2 pulsations with harmonious H oscillations and discrete D bays in the sub-aurora zone suggest a common source with diverse tunneling paths. Scalograms of Pi-2 undulations of the frequency band of 6.7-22 mHz were observed despite different kinds of Pi-2s. Auroral Pi-2s were highly localized in local time with clear H and D bays, implying magnetospheric-ionospheric current couplings. Latitudinal and longitudinal Pi-2 propagations are exemplified by 180° phase-shift (polarization) in EWA and group delay in the mid-latitudes of the northern hemisphere. Overall, Pi-2 wave power from high to low latitudes declined with peak amplitudes of 15 nT to less than 1 nT, respectively. Finally, external influences from sea currents causing signal attenuation due to the station's proximity to the sea were also identified. To conclude, the accuracy and efficiency of wavelet analysis with no computation hassle render it a valuable tool for the study of space events in the magnetospheric community.

1 Introduction

Pi-2 pulsations are transient, irregular geomagnetic oscillations with periods ranging from 40 s to 150 s (Singer et al., 1983). These magnetohydrodynamic waves are usually observed at the onset of substorm expansions and auroral breakups (Sakurai & Saito, 1976). One remarkable property of Pi-2 undulations is their extensive spatial distributions. They span from local magnetic time (MLT) and/or invariable latitudes to global events covering many hours of MLT extending from low to high latitudes. This spatial variability is believed to reflect different Pi-2s generation mechanisms (e.g., Keiling & Takahashi, 2011). Studies based on observations have illustrated that Pi-2 pulsations monitored on the ground consist of superpositions of different components (Yumoto et al., 2001). At low latitudes, the Pi-2 beats observed at different latitudes and longitudes occur with a common waveform and frequency(Sutcliffe & Yumoto, 1991). Recent studies suggest these low-latitude Pi-2 pulsations are generated by cavity resonances excited by earthward-propagating fast mode waves launched at substorm commencement(Yumoto, 1990; Takahashi et al., 1995; Allan et al., 1996; Kepko et al., 2001; Hsu et al., 2012). In contrast, mid-latitude Pi-2 pulsations are believed to originate from the disturbance of cross-tail current associated with Alfven waves carrying field-aligned currents, which play a role in the substorm current wedge establishment (Sakurai & Saito, 1976).

Statistical studies on space and ground-based Pi-2 pulsations indicated that regions inside the inner magnetosphere (L = 2 to 5) 3 hours past their local midnight are dominated by poloidal components such as compressional (Bz) and radial (Bx). These components correspond to fast mode waves polarized in the direction of their Meridian (Baumjohann & Glaßmeier, 1984). Global Pi-2 oscillations, alternatively, are the result of plasmaspheric cavity resonance (PCR), a system eigenmode of the plasmasphere (e.g., Yeoman & Orr, 1989; Lin et al., 1991; Takahashi et al., 1995). Since PCR is restricted to plasmaspheric field lines, any adjustment of the PCR leads to the emergence of wave energy in the plasma sheet, effectively escaping from the plasmasphere. Lee and Lysak (1999) defined this phenomenon as plasmaspheric virtual resonance (PVR) (Takahashi et al., 2003; Teramoto et al., 2008). In the PVR model, it is argued that the decrease in the Pi-2 amplitudes occurs outside the plasmasphere (Takahashi et al., 2003). Typically, related oscillation periods are longer than those of the PCR/PVR-Pi-2s (Baumjohann & Glaßmeier, 1984)

and their largest amplitudes lie in the auroral zone, specifically at high latitudes(Samson, 1982).

The timing issue of Pi-2 pulsation from the polar cap to the magnetic equator was conducted by Uozumi et al. (2000). Uozumi et al. (2000) addressed the timing relation to Pi-2 power obtained from the oscillation of the H component. They investigated the relationships between the relative timing of the maximum amplitude of Pi-2 magnetic energy and the latitudinal propagation of Pi-2 perturbations. In their finding, the timing of the maximum power implied the group velocity or group delay, which was used for the examination of the wave energy transfer of Pi-2 pulsations. However, they did not look into the characteristics of longitudinal Pi-2 wave propagation. Uozumi et al. (2004) used the Uozumi et al. (2000) approach to address the characteristics of longitudinal and latitudinal Pi-2 propagation in the auroral zone. The morphology of Pi-2 propagation in high-latitude areas was determined. Nevertheless, this morphology was limited to high-latitude areas and thus, it was insufficient to fully explain Pi-2 propagation on a global scale. Uozumi et al. (2009) clarified the low-latitude and high-latitude timing relations by MLT dependence of the delay time of the auroral Pi-2 for each horizontal component utilizing the low-latitude Pi-2 timing as a reference. The propagation and generation mechanism of these plasma waves is still ongoing. The current study briefly addresses the timing issue by considering both postmidnight and pre-midnight Pi-2 ULF waves globally.

Ground Pi-2 pulsations are composed of several different modal components (Fukunishi, 1975). It is, however, principally challenging to decompose the mixed waveform using the conventional Fourier transform method because of the overlapping frequency ranges. The locality and complexity of natural signals require robust tools to explore their hidden patterns and detect their presence in raw settings. The rapid fluctuation in the phase and frequency of waves poses another challenge. Hence, it is important to introduce techniques that make it possible to separate such mixed signals into individual modal components as ground-observed Pi-2 pulsations. The multifrequency analysis criterion accurately characterizes the time-frequency component of natural signals while preserving their original formation. Therefore, it is a desirable tool for events associated with space activities and wave analysis in general. Wavelet is a powerful analytical tool in the fields of space science, acoustic industry, mathematics, and many other economic sectors. The power of Wavelet to resolve time-frequency resolution measurements and detect intelligence in signals from noise-masked signals with minimum computation power motivated its selection (yang Zeng & guang Wang, 2013).

Wavelet transform applications in space sciences have succeeded significantly in studies of space events. It has been widely used in the denoising of geomagnetic field data (Kumar & Foufoula-Georgiou, 1997; Jach et al., 2006; Xu et al., 2008), the geomagnetic storm initial phase determination (Hafez et al., 2010), the automatic detection of sudden storm geomagnetic onsets (Hafez et al., 2012), in the automatic recognition of Pc5 and Pc3 pulsations using machine learning (Omondi et al., 2023b; Balasis et al., 2019) and the extraction of periodic components caused by the rotation of the Earth. This paper focuses on the automatic detection of Pi-2 pulsations from the ground magnetic field variations associated with the explosive plasma phenomena of auroral substorms. In practice, without pre-determining any modes or frequency range as the norms in the Fourier transform, the wavelet automatically distinguishes anomalies from Pi-2 with no signal distortion (Vetterli, 1986). The wavelet power manifests itself in the ONW data when Pi-2 pulsations are recovered from modulation from sea currents because of the proximity of the ground monitor to the sea. Finally, the causality of Pi-2 ellipticities, time delays, and longitudinal propagation during substorm onset are also investigated. The current paper is organized into five major sections, beginning with the introduction, followed by data and methods, then results, summary and discussion, and finally conclusion.

2 Data and Methods

Our study analyzes the data from the ground-based magnetometer stations in the Circum-pan Pacific Magnetometer Network (CPMN) along 210° magnetic meridians (MM) chain. The data measurements were done by magnetometers as described on the MAGDAS website (`https://data.i-spes.kyushu-u.ac.jp`). In the study, data from 15 monitors were used for Pi-2 pulsation detections (refer to Figure 1 and Table 1). The data sets presented were in unprocessed settings dominated by noise, with ZYK and KOT recording the worst. White noise was dominant in many stations. These noises can be effectively eliminated by the proper application of conventional methods such as low-pass filtering at a given cut-off frequency which requires careful evaluation to perform. These methods have drawbacks and perhaps lead to signal loss in the process of data wrangling. The power of wavelet manifests in signal detection in the presence of noise-infested data. It performs excellently well in anomaly detection and signal discrimination with nearly the same frequency band as the case of the Pi-2 and Pc-4 classes. The two phenomena are related in time-frequency property with different physical oscillation, occurrence duration, and signal energy. Pc-4 for instance is continuous, long occurrence duration, and is linked to different space phenomena occurring outside the inner magnetosphere. While Pi-2 portrays completely different signal aspects suited for inner/outer magnetospheric studies. Using wavelet analytics does not necessarily require much data remediation aside from basic data munging such as formatting or parsing to ensure data is human-machine readable. Table 1 lists CPMN stations and their respective coordinates in both geographic and geomagnetic systems. Where abbreviations; Glat and Glon are the geographic latitude and longitude while GMlat and GMlon are the geomagnetic latitude and longitude respectively. Finally, L is the L-shell value for each respective station.

Table 1. List of CPMN Ground Stations along 210° magnetic meridian

Station	GLat (°)	GLon (°)	GMLat (°)	GMLon (°)	L
KTN	75.94	137.71	69.92	201.03	8.62
TIK	71.59	128.78	65.65	196.90	5.98
CHD	70.62	147.89	64.66	212.14	5.55
ZYK	65.75	150.78	59.60	216.76	3.97
MGD	59.97	150.86	53.49	218.75	2.87
PTK	52.94	158.25	46.17	226.02	2.12
ONW	38.43	141.47	31.15	212.63	1.39
KAG	31.58	130.72	24.37	202.36	1.22
GUA	13.58	144.87	5.61	215.55	1.03
BIK	-1.08	136.05	-9.73	207.39	1.05
EWA	21.32	-158.00	21.63	269.45	1.18
KOT	66.88	-162.60	64.52	249.85	5.49
WEP	-12.68	141.88	-21.93	214.44	1.18
BSV	-25.54	139.21	-36.10	213.08	1.56
CAN	-35.30	149	-45.72	226.29	2.08

In the current study, 1 s data cadence was used for 30 minutes consisted in all stations. This time window was logical for Pi-2 analysis which only happens for a period between 10-15 minutes. Furthermore, the data used for Pi-2 oscillations analysis in the work corresponding to the substorm onsets period occurred at 22.97 MLT, 17th, February 1995 and observed in the geographic location 70.2°, 147.89° (`https://supermag.jhuapl.edu/substorms/`). The substorm onset events of the February 17th were obtained from the Forsyth et al. (2015) substorm onset list. According to the SOPHIE technique, the onset occurred at 13:39 UTC. The topographical map in Figure 1 gives information about

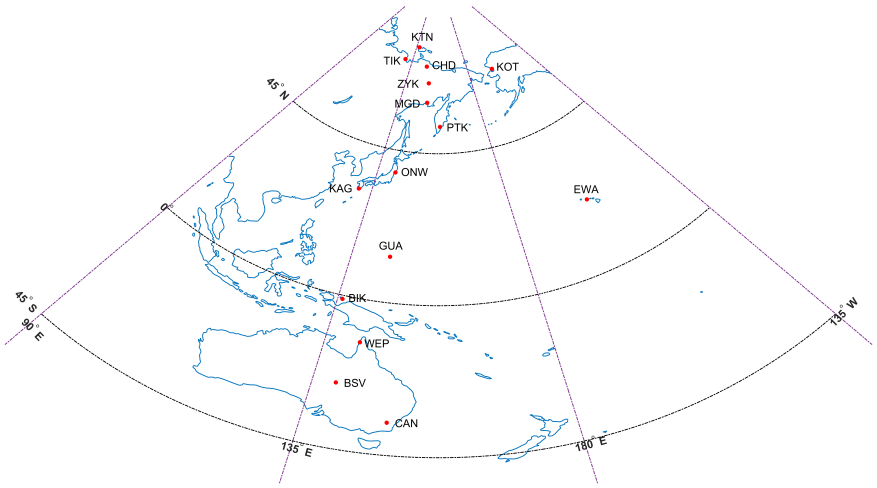

Figure 1. The topographical map of the 210° magnetic meridian MAGDAS magnetometer stations. The latitude and Longitude in the map are expressed in the geodesic coordinate system.

the location of each CPMN station. This CPMN network gives the global view of these Pi-2 ULF wave distributions, the latitudinal wave propagation, and the evolution from Pi-2. The stations' exact locations on the map are marked with red stars.

2.1 Wavelet Analysis

Ground geomagnetic field measurements often consist of many physical component embeddings such as dipole field and perturbations from space. The study of each embed in isolation on the same scale as the original signal requires multiscale approximation or multiresolution analysis. This refers to signal decomposition into individual components in different scales and upon reconstruction can produce the exact single signal as the original signal. Wavelet analysis techniques utilize this method in the detection cases using discrete wavelet transform. Mathematically, ground magnetic perturbations in the realm of wavelet analytics can be conceptualized as follows. Consider a function $f(t)$ as the original signal. If $f(t)$ is a series of approximations of subspaces such that $f(t) \in V_j$ where j is the integer of increasing values, then $f(2t) \in V_{j+1}$. Projecting the function $f(t)$ at each level j onto the subspace V_j, the projection then is defined by the approximation coefficient $C_j[l]$. The inner product of $f(t)$ with the translated and dilated-scaled version of the scaling function $\phi(t)$ is given by Eq.1 (S. G. Mallat, 1989):

$$C_j[l] = \langle f, \phi_{j,l} \rangle = \langle f, 2^{-j}\phi(2^{-j} \cdot -l) \rangle \tag{1}$$

where the scaling function, $\phi(t)$, satisfies the condition described in Eq.2.

$$\frac{1}{2}\phi(\frac{1}{2}t) = \sum_k h(k)\phi(t-k) \tag{2}$$

The expression in Eq.2 permits the direct computation of C_{j+1} from C_j. From C_0 all the coefficients $(C_j[l])_{j>0,l}$ can be calculated without directly invoking any other inner product:

$$C_{j+1}[l] = \sum_k h(k-2l)C_j[k] \tag{3}$$

The number of inner products at each level j is divided by 2. Gradually the signal is smoothed leading to loss of information. The details (low-pass signal) are recovered from the subspace W_{j+1}, which is the orthogonal component of V_{j+1} in V_j. This subspace is generated using wavelet function $\psi(t)$ by dilation and translation (Daubechies, 1988, 1992;

S. Mallat, 2009).

$$\frac{1}{2}\psi(\frac{1}{2}t) = \sum_k g[k]\phi(t-k) \tag{4}$$

The wavelet coefficients are calculated by Eq.5-6

$$\begin{aligned} W_{j+1}[l] = \langle f, \psi_{j+1,l}\rangle &= \langle f, 2^{-(j+1)}\psi(2^{-(j+1)})\cdot -l\rangle \\ &= \sum_k g(k-2l)C_j[k] \end{aligned} \tag{5}$$

$$\begin{aligned} C_{j+1} &= \left[\tilde{h} \star C_j\right] \downarrow_2 \\ W_{j+1} &= \left[\tilde{g} \star C_j\right] \downarrow_2 \end{aligned} \tag{6}$$

To recover the original data, we utilize the properties of orthogonal wavelets. Considering biorthogonal wavelet bases filters $\tilde{g}$ and $\tilde{h}$ (Cohen et al., 1992) are defined to be dual to g and h such that (g, h, $\tilde{g}$, $\tilde{h}$) gives a perfect reconstruction filter bank. Then, the reconstruction of the signal is performed by expression

$$\begin{aligned} C_j[l] = 2\sum_k \left(\tilde{h}[k+2l]C_{j+1}[k] + \tilde{g}[k+2l]W_{j+1}[k]\right) \\ = 2(\tilde{h} \star \tilde{C}_{j+1} + \tilde{g} \star \tilde{W}_{j+1})[l] \end{aligned} \tag{7}$$

where $\tilde{C}_{j+1}$ is zero interpolation of C_{j+1} given by the assertions

$$\begin{aligned} \tilde{C}_{j+1}[l] &= \left[C_{j+1}\right] \uparrow_2 [l] \\ &= \begin{cases} C_{j+1}[m] & \text{if l=2m} \\ 0 & \text{Otherwise} \end{cases} \end{aligned}$$

and the filters $\tilde{g}$ and $\tilde{h}$ must verify the biorthogonal conditions of de-aliasing and exact reconstruction (Vetterli, 1986). Equation 1 to 7 describes the formulations of wavelet multiresolution analysis. Where Morlet continuous wavelet transform and coherence were formulated using the same concept demonstrated in my previous publication(Omondi et al., 2023a).

In the study, we utilized a 1-dimensional multiresolution wavelet decomposition method to decompose data into wavelet decomposition vector v and bookkeeping vector b using level 5 Daubechies wavelet of order 8 (Daubechies, 1992; S. G. Mallat, 1989). To obtain signals, the 1-D wavelet reconstruction method was performed with the v,b, and db8 as the input to the wavelet reconstruction function. In principle, only two signals were possible to reconstruct, that is, the high-frequency component also known as approximations, and the low-frequency counterpart called details. Details were explicitly obtained by specifying the command 'd' as the first input of the wavelet reconstruction function. This is the intelligible waveforms in the spectrum of Pi-2 waves. This step was repeated to reproduce background information as an approximation replacing 'a' in place of 'd' (Daubechies, 1992; Omondi et al., 2023b). Figure 2 & 3 gives vivid visual steps and results of the wavelet analysis technique explored.

Figure 2 summarises Pi-2 pulsation detection processes schematically using pure raw data as the input. For validation of the accuracy of the detection signal, we used the Morlet wavelet to observe the frequency-time property of the Pi-2 pulsations as shown in Figure 2 & 4, for example, (Omondi et al., 2023a, 2023b). The picture of Daubechies wavelet transform as an automatic detection tool was explicitly demonstrated in Figure

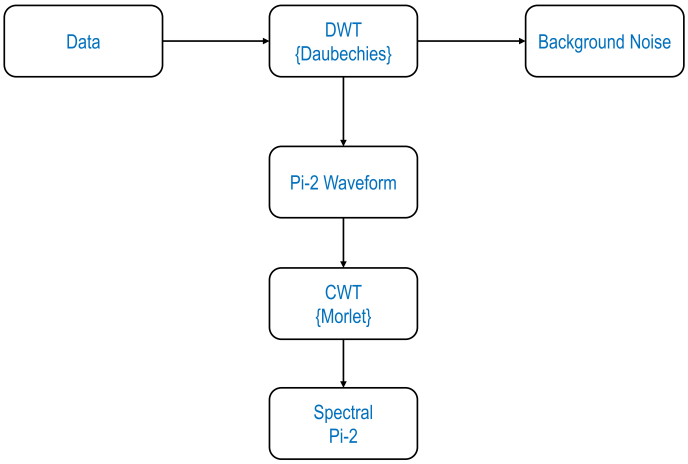

Figure 2. Schematic flowchart diagram illustrating successive stages of Pi-2 pulsation detection using wavelet detection criterion from magnetic field data.

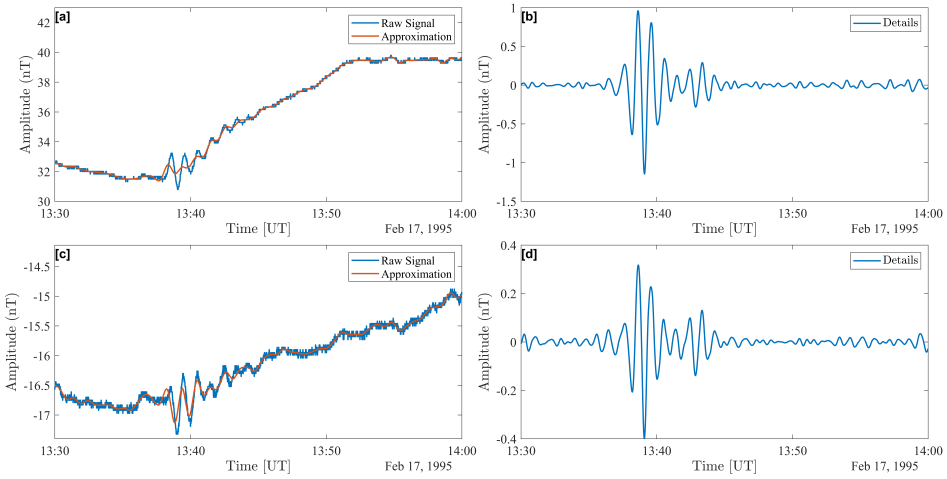

Figure 3. Time series plots of the horizontal component of the magnetic field, the raw data in blue and approximation in orange. Panels (a) & (b) are examinations from CAN and (c) & (d) are from the EWA station. The details and approximation are Pi-2 pulsations and background noise respectively.

3, taking CAN and EWA station H-components as illustrative cases. Where the observations in (a) & (b) are from CAN and (c) & (d) from EWA respectively. Figure 3 (a) & (c) shows the raw magnetic field data in blue and the approximation in orange after wavelet decomposition and reconstruction. The detected Pi-2 waves are shown in Figure 3 (b) & (d). Where UT is the abbreviation for universal time. We can see approximations in panels 3(a) & (c) are highly smoothed and deviate from the raw data having similar trends. It is important to note that this approximation contains many sig-

nal components except one extracted at level 5. These signals are not in the scope of this study and any oscillatory studies such as Pi-1 or Pc3-4 may be present in it and are treated as background noise. The vivid dominant white noise seen in panels 3(a) & (c) can be obtained explicitly by the wavelet analytic denoising method as demonstrated in my previous publication (Omondi et al., 2023b).

3 Results

The classification scheme for observed ground Pi-2 pulsations using latitudinal extents: low, mid, and high latitudes are unclear, and the L-range based division alone is also insufficient (Sutcliffe & Yumoto, 1989). Hence, accounting for Pi-2 pulsations covering more than one L range is highly desirable. The preferred categorization scheme for Pi-2 waves on their physical properties is one proposed by Samson (1982), defining high latitudes as any region influenced by magnetic fields from the ionospheric substorm electrojet. The regions situated latitudinally below are termed mid-latitude regions. This definition gives freedom for the latitudinal motion of the electrojet with geomagnetic conditions. This paper adopted this convention, referring to high latitude ground Pi-2 pulsations as auroral zone Pi-2, and the equatorward as sub-auroral zone Pi-2 (Yeoman & Orr, 1989). With this definition, the plasma sheet field lines are accurately mapped as conjugate to the auroral zone, and the plasma trough and possibly portions of the plasmasphere as a mirror of the sub-auroral zone. The low latitude zones are retained as regions with $L < 2$. The scalograms in Figure 4,5,6,9 and 10 are the automatically detected Pi-2 pulsations by Morlet mother wavelet continuous transformation of the Daubechies discrete wavelet transform (waveforms) from the magnetic field lines of the CPMN stations.

3.1 Sub-Auroral Pi-2 Pulsations

Figures 4-6 illustrate global Pi-2 oscillations in low-latitude observed in the nightside sector. Each panel shows results obtained from the H and D magnetic field components in the corresponding stations in local time (LT). Overall, Pi-2 pulsations recorded in the magnetic field H component in all mid-low latitude stations (Fig. 8) arrived simultaneously with a clear coherent profile suggesting the same wave originating from the same source. Compared to those monitored in the D component, they arrived at different times. Demonstrating interesting findings about the Pi-2 waves and their propagation mechanisms in the magnetosphere during geomagnetic activity along 210° MM. The wavelet scalograms in Figures 4-6 show Pi-2 pulsation of frequency range 6.7-22 mHz consistent in all stations.

Figure 4 presents observations in BIK, GUA, and EWA stations with L-shell values of 1.03 and 1.13 respectively. BIK and GUA are conjugate stations located in opposite hemispheres sharing similar L-values and nearly the same local time. Panels 4(a)-(c) and 4(d)-(f) are Pi-2s detections from the H and D components. The examination of the H component showed clear short transient pulses of damped oscillations with higher amplitudes maximum between 0.3 and 1.5 nT while the D component recorded 0.1 and 0.3 nT spread across three stations. Furthermore, the ULF wave signature in the D panels showed distinct waveform profiles in each station vividly illustrated in scalograms 4(d), (e), and (f). Surprisingly, all the H-components in the three stations oscillated in phase despite their 4-hour difference in local time. The scalograms in H were short-lived compared to the D component in the GUA & BIK observatory. On the contrary, at EWA station which is 1 hour to midnight, smaller waveforms by a factor 5 were detected in both components and were 180° phase shifted in H and D. EWA also recorded similar scalograms as demonstrated in Figure 4(c) & (f). This indicates the localization of Pi-2 pulsation power to a local time. Detailed analysis on Pi-2s polarizations at EWA station is shown in Figure 7.

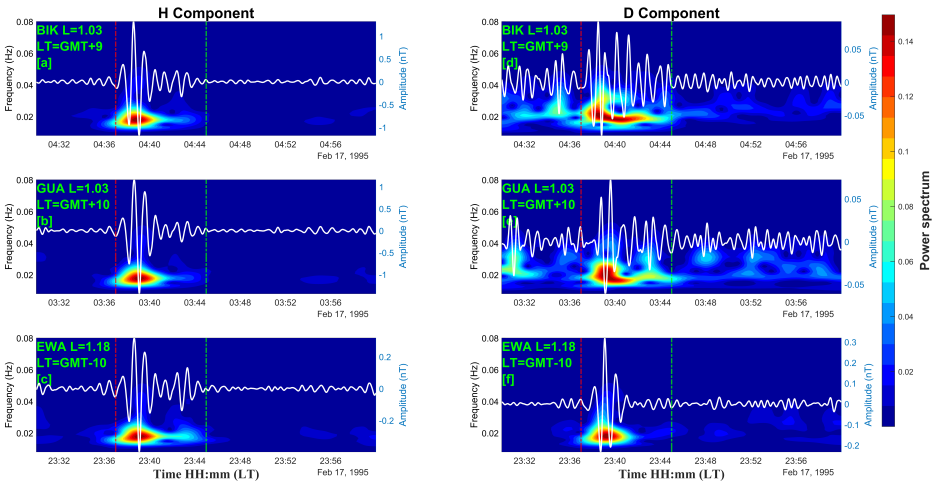

Figure 4. Low latitude Pi-2 pulsation detected BIK, GUA, and EWA. Where (a), (b) & (c) and (d), (e) & (f) are Pi-2 waves recorded in H and D components respectively. The white solid waveform & scalogram are Pi-2 pulsations and the red & green dashed line is Pi-2 duration.

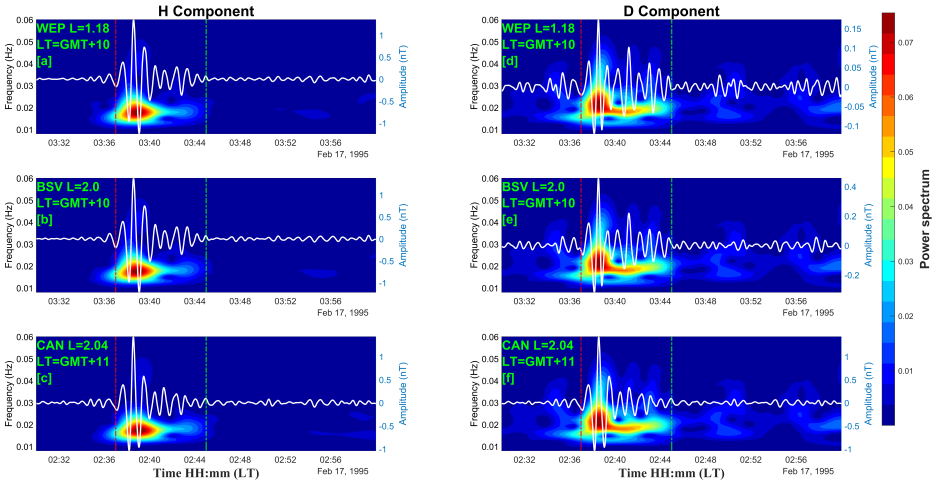

Figure 5. Low Latitude Pi-2 pulsation detected in WEP, BSV, and CAN ground monitors. Where (a), (b) & (c) and (d), (e) & (f) are Pi-2s in H and D components respectively. The white solid waveform & scalogram are Pi-2 pulsations and the red & green dashed line is Pi-2 duration.

Figure 5 demonstrate a special case of Pi-2 waves recorded in WEP, BSV, and CAN stations located in L=1.18, 2.0, and 2.04 respectively. The wave trains in H and D arrived at the same time with coherent wave bays which are in phase at WEP, BSV, and CAN. The Pi-2 wave amplitudes in D magnetic field components are smaller in magnitude in the order of a tenth to those in H at WEP and BSV stations. The Pi-2 profiles in both components are distinct with scalograms in the H component being short while those in D elongated. This invites an interesting question; why would observatories in low to mid-latitude stations located southern hemisphere report unique findings compared to their counterparts? The possibility of Pi-2 source initiation origin and the prop-

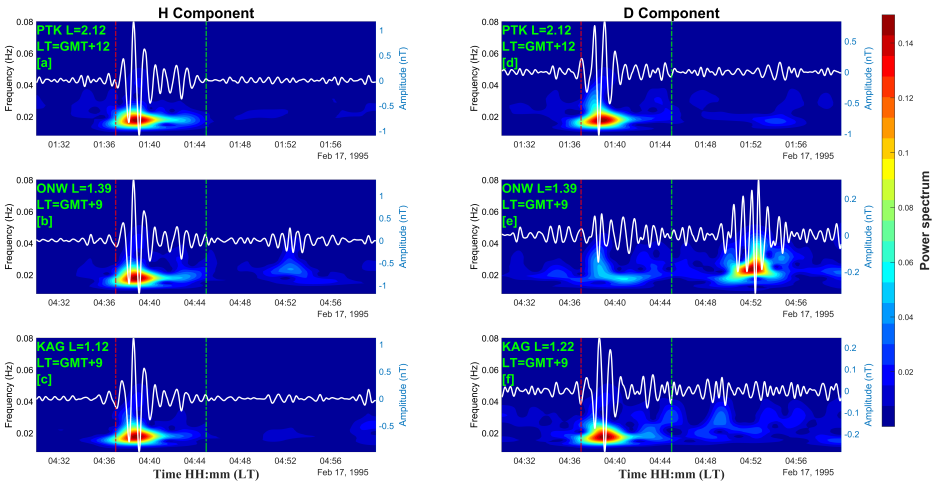

Figure 6. Mid and low-latitude Pi-2 pulsation record from H and D magnetic field components. The KAG, ONW, and PTK stations show comparative observation of Pi-2 oscillations in H and D components in (a)-(f). The red and green dashed lines correspond to the detected Pi-2 Pulsations

agation media perhaps are directly linked to this observation. The northern auroral zone stands to be a location where Pi-2 originated and was more disturbed as Pi-2s are distributed along 210 MM globally.

Figure 6 shows the observations from the PTK, ONW, and KAG observatories in their local time with L-values 2.12, 1.39, and 1.12 respectively. The wave response on the H component arrives simultaneously with the same wave bays in all stations. All wave profiles in the D component are reversed. Dominance of external effects such as local sea currents heavily attenuated the signal arriving at the ONW station in the D component. Hence, results in weak Pi-2 signal reception on the azimuthal component as illustrated in the waveform and scalogram. The Pi-2 pulsation was modulated by the sea currents due to ONW's proximity to the sea (e.g., Romero et al., 2020). It was noted that Pi-2 power dominated more on the H as the D component was severely attenuated and more likely modulated by local effects. Regardless, the recovered signal in D showed a similar pattern in all three stations. It was uniquely observed that Pi-2 waves in both magnetic components were 180° out of phase with H having a higher amplitude than those in D. This implies that the latitudinal profiles of Pi-2 perturbation consist of different mode oscillations.

Pi-2 wave evolution and polarization in H and D magnetic field components during pre-substorm, substorm onset, and post-substorm periods in EWA stations are shown in Figure 7. In the pre-substorm and post-substorm periods, the Pi-2 signal arrived at EWA with a slight phase difference in both components with the H leading as shown in R1 & R2 of Figure 7(a). In the substorm expansion phase, the Pi-2 oscillations evolved with 180° out of phase as in R3 with a peak amplitude at 23:39 LT. This is demonstrated by the horizontal arrows panel 7(b) corresponding to a phase shift of π projected in a unit circle. This polarisation lasted for about 10 minutes. There were similar observations in the PTK, ONW, and KAG in reverse (Fig. 6). Time-frequency consistency and phase difference of Pi-2 pulsations illustrated in Figure 7(b) were consistent with observations demonstrated in Figure 7(a). The small arrows in phase-frequency coherence analysis in Figure 7(b) represent the phase angle between the two signals. The H and D demon-

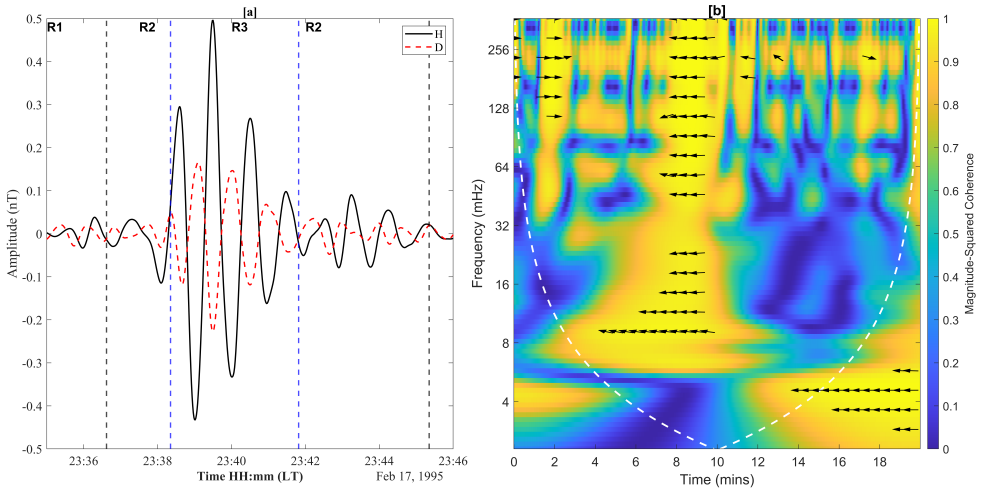

consistent

Figure 7. Pi-2 Pulsation observed in H and D components from EWA ground monitor. (a) illustrates the Pi-2 phase shift and evolution between two magnetic components. (b) shows the wavelet frequency and phase coherence of signals in (a). Where Pi-2 ripples from H and D are in a black solid line and a red dashed line respectively. The blue and black vertical dashed lines show the partition between the region of Pi-2 wave evolution marked by R1, R2, and R3. Finally, the black arrows in panel (b) show phase shift. In principle, vertical arrows show phase lag on a unit circle corresponding to a $\frac{\pi}{2}$. Therefore, the corresponding phase lag of π in panel (b) is consistent with that in panel (a).

strated a high-frequency coherence in the substorm expansion period lasting for 10 minutes beginning from the second minute from the left of panel 7(b).

Figure 8 illustrates the physical properties of Pi-2 wave trains detected in middle and low-latitude stations along 210° MM. In Figure 8 (a) all Pi-2 oscillations beating these regions showed similar wave profiles. These oscillations arrived at 13:37 UT peaking at 13:39:11 UT and gradually decayed. The observations in Figure 8 (b) show that the ultra-low frequency waves of the Pi-2 type delayed arriving at different times in some stations. These D-component waves showed different properties with some peaking simultaneously earlier while some later taking 13:37 UT as the arrival time with CAN and PTK as reference. This unique feature hints at the magnetospheric structure and wave propagation time. To visualize the underlying unique properties of the Pi-2 undulation in Figure 8. The latitude dependence of the Pi-2 pulsations picture and patterns are projected in Figure 8(b).

3.2 Auroral Pi-2 Pulsations

Figures 9 and 10 illustrate nightside Pi-2 undulations observed in the auroral zone. Figure 9 presents the observations in the ZYK, MGD, and KOT stations located at L = 3.97, L = 2.87, and L = 5.41, respectively. There was a phase shift in observations between ZYK and MGD ground monitors as well as in their components despite sharing the same local time. From Table 1 we note ZYK is east of MGD. The negative D oscillations indicate the center of the substorm current wedge is located west of these two monitors(Clauer & McPherron, 1974). The positive H at MGD implies that the downward field-aligned current section of the wedge is situated east of the station. Focusing

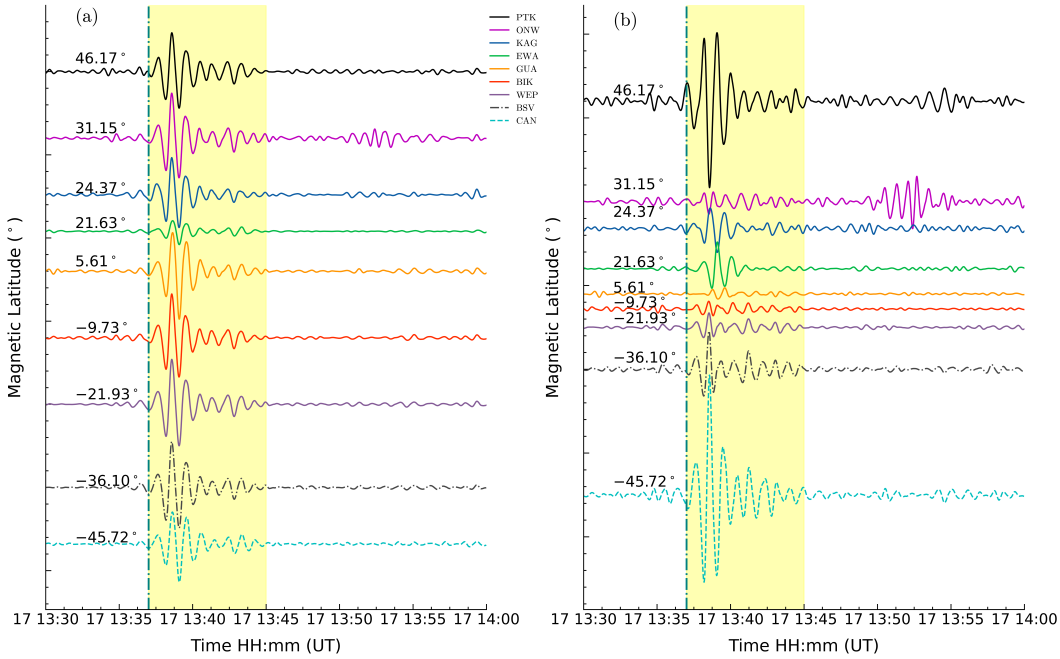

Figure 8. Sub-auroral Pi-2 pulsation waveforms. (a) and (b) shows the H and D perturbations respectively. The H component responded with similar Pi-2 waveforms and amplitude spanning from -45.72° to 46.17° magnetic latitude except for EWA and all peaking at 13:39:11 UT. Similarly, the D component recorded the same waveform in the northern hemisphere stations(46.17°, 31.15°,24.37° & 5.61°) except 21.63° while waves in the southern hemisphere phase reversed in D peaking at 13:38:42 UT. Teal dashed-dotted lines correspond to the detected Pi-2 Pulsations onset while the faint yellow shade is the Pi-2s duration.

on ZYK, Pi-2 ripples arrive delayed by 2 minutes in both magnetic components with a phase reversal of 180°. The ZYK and KOT stations recorded high Pi-2 pulsations amplitudes in both magnetic components with ZYK having 2 nT and KOT 6 nT in the horizontal magnetic component and 1 nT and 2 nT in the D components respectively. MGD responded similarly to those in midlatitude zones with enhanced Pi-2 wave amplitude of 1.5 nT and 1 nT in H and D respectively. In the auroral zone, Pi-2s were observed in KTN, TIK, and CHD observatories located at L=8.62, 5.98, and 5.55 respectively. Figure 10 illustrates the examinations in H and D magnetic components. whereby, Pi-2 oscillations presented various wave profiles localized in each observatory and were completely different from those observed in the sub-auroral regions. Furthermore, the wave morphology scalograms were unique in the three stations both in H and D magnetic field components. Therefore, probably suggests that the wave source and propagation medium are unique and localized for each region. The three wave signals arrived at different times for both components as shown in Figure 10. The wave amplitude in the KTN H panel is twice that in the D panel. TIK recorded a maximum of 5 nT and -4 nT in amplitudes while CHD 5 nT and -10 nT respectively. Overall, all signals presented different spectra, scalograms and with -10 nT and 15 nT peak amplitudes. Figure 11 describes the Pi-2 wave profile in mid-high magnetic latitude. It was observed that the wave profile evolves as it propagates from the auroral to the sub-auroral zone. This wave evolution is visible in all frequencies and amplitude in both magnetic field components signifying the nature of their propagation path in the magnetosphere and ionosphere. Amplitude changes are well shown in Figure 12. The latitudinal and amplitude relationship of Pi-2 magnetohydrodynamic waves globally are illustrated in Figure 12. These observations,

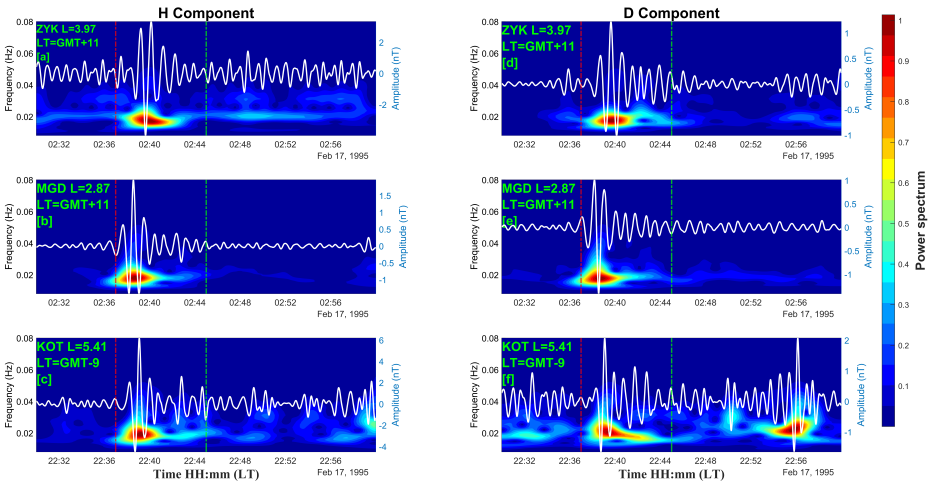

Figure 9. Mid-high latitude Nightside Pi-2 pulsation detected in ZYK, MGD, and KOT stations in H and D components. The red and green dashed lines show the span of detected Pi-2 pulsations.

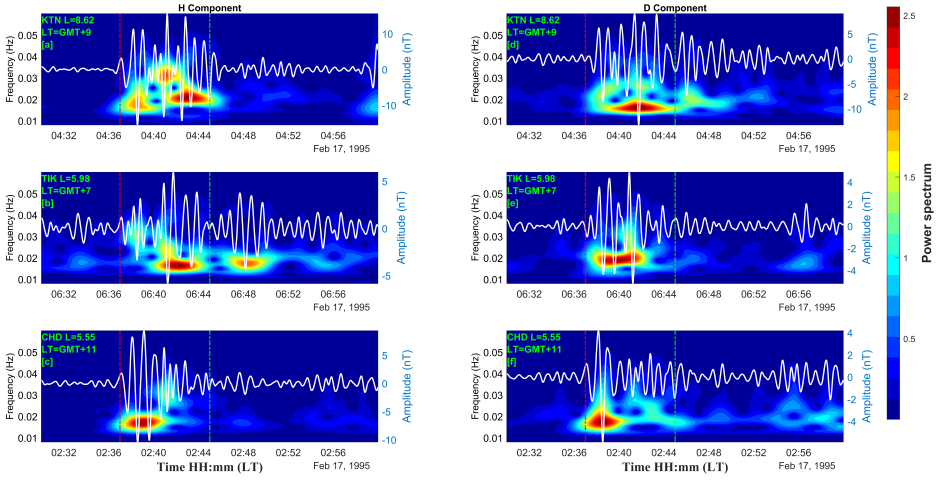

Figure 10. High latitude Pi-2 pulsation detected in KTN, TIK, and CHD stations in H and D components. The red and green dashed lines correspond to the detected Pi-2 Pulsations.

present global wave activities in the H and D components of the magnetic fields. Generally, there was a gradual decrease in Pi-2 pulsation activities equatorward from the zones of auroral brightness intensification along 210° MM. The sharp break in the trend accompanied by an increase in amplitude at CHD compared to TIK indicates a bizarre activity interesting for this study. Overall, The Horizontal component in all latitudes responded with high amplitudes compared to the D components.

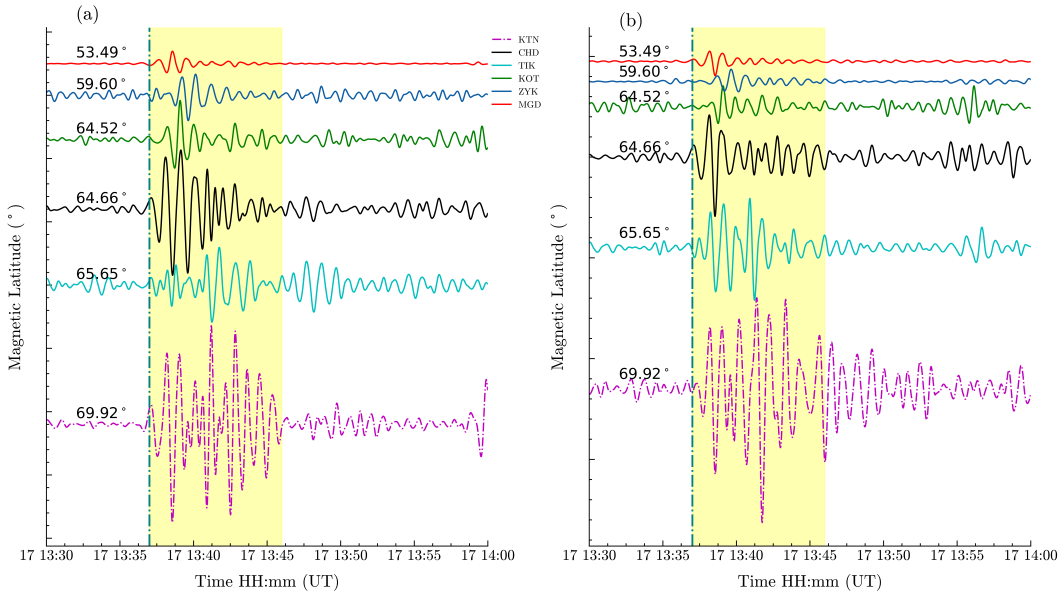

Figure 11. High and mid latitude Pi-2 pulsation waveforms. (a) and (b) shows the H and D perturbations respectively. Collectively, all Pi-2 ULF waves monitored in high latitudes exhibited different wave profiles. Teal dashed-dotted lines correspond to the detected Pi-2 Pulsations onset while the faint yellow shade is the Pi-2s duration.

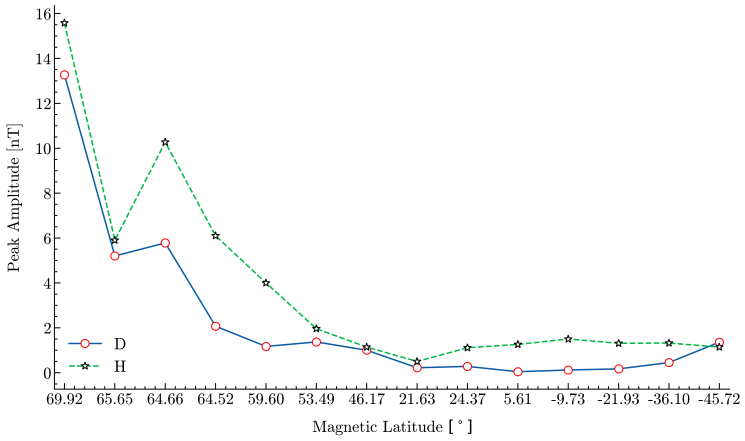

Figure 12. Latitudinal profile of Pi-2 amplitude along 210° MM. Pi-2 absolute amplitude decreases with the decline in absolute magnetic latitude.

4 Summary and Discussion

The characteristics of Pi-2 pulsations observed in the auroral to sub-auroral zone using ground magnetometer data obtained from the CPMN along 210° MM were carefully analyzed. The low-latitude Pi-2 pulsations arrived at 13:37:00 UT, 2 minutes earlier in most observatories in both hemispheres compared to the predicted time of substorm onset, 13:39:00 UT. Consequently, similar observations in H-components of KTN and CHD observatories were detected. These high correlation global Pi-2 events monitored on the nightside in a wide latitudinal and narrow magnetic meridian constituted highly consistent waveforms. Similarly, the same observations were also reported by Keiling et al. (2014a); Uozumi et al. (2009, 2011, 2016a) on their work. Uozumi et al. (2009) stud-

ies on high latitude in the pre-midnight sector resolve to a similar systematic delay in horizontal components and strong Pi-2 pulsations MLT dependence. These wave properties in the auroral zone are strong indicators of forced Alfven waves excited by fast magnetosonic waves (Uozumi et al., 2009). However, the Observatories such as TIK and ZYK exhibited a common time delay of about 2 minutes in their H components compared to those in the low-latitude stations (refer Figure 8 and 11). The delay in Pi-2 arrival in the auroral zone is due to differences in mode conversion and distinct propagation paths. Fast mode waves propagating in the azimuthal direction in the magnetosphere can excite field-aligned mode waves(Alfven waves) on the field lines away from the source region as in the case of the KOT station.

The underlying relationship between KTN, CHD, and ZYK to low latitude ground monitors in terms of observed Pi-2 wave properties is complex. In other studies, however, global Pi-2 pulsations have a single period, while spanning the equatorial to auroral zone with their largest amplitude at high latitudes. This implies that their source lies beyond the plasmasphere (outer magnetosphere). Therefore, to distinguish these waves from the global Pi-2 associated with the global PCR/PVR-Pi-2 pulsations types, they are named super global Pi-2s. The source generation mechanism differentiates super global Pi-2s from Pi-2s types with different periods occurring simultaneously from low to high latitudes. Li et al. (1998) reported Pi-2 events that displayed two periods at different latitudes and argued that the transient response mechanism operated in the high latitudes while PCR in the low and mid-latitudes (Keiling et al., 2014b). However, for super global Pi-2, it was suggested that only one generation mechanism operated, even if with numerous different propagation conduits from their source to the ground(e.g., Uozumi et al., 2009). On the other hand, sub-auroral global Pi-2 pulsations have also been explained initially by cavity resonance(Takahashi et al., 1999). It was pointed out that in principle, these Pi-2 waves are triggered by forced driving of the system. Other observational evidence on the forcing mechanism argued that the observed sub-auroral Pi-2 oscillations were driven by velocity modulations in fast plasma flows (BBF) in the central plasma sheet, which would subsequently couple to MHD waves in the plasmasphere (inner magnetosphere). Keiling et al. (2008) proposed high-latitude forcing showing evidence that some ground Pi-2 waves are directly controlled by the reconnection site also known as reconnection-driven Pi-2 pulsations. While the source for the BBF-driven Pi-2s is connected to tail reconnection. Thus, the propagation model must be different compared to that of the reconnection-driven Pi-2 model. The latter suggested that besides the flow modulations in the plasma sheet, Alfvénic variation on high-latitude flux tubes carried the Pi-2 signal faster to high latitudes on the ground, where Pi-2s were first spotted. Therefore, associating monochromatic Pi-2 pulsations observed in the sub-auroral as super global Pi-2 is logical.

The phase reversal (180 ° out of phase) between ZYK and CHD with corresponding L-values of 3.97 and 5.55 indicates the plasmapause location. For certainty, this observation syncs with Tokunaga et al. (2007) results showing they are probably situated along the plasmapause boundary during the Pi-2 pulsation event. Polarization reversal of substorm-related Pi-2 undulations near plasmapause has been generally accepted by many researchers (e.g., Fukunishi, 1975). Takahashi et al. (2003) described the events occurring near the plasmapause at CRRES (Combined Release and Radiation Effects Satellite) using the phase of compressional component (Bz) to be assembled both at 0 ° and 180 °. Their observations pointed out a consistent trend with the cavity mode according to a numerical simulation using a realistic plasmapause plasma density structure and a dipole magnetic field, which shows that the node of Bz is situated near the plasmapause. CHD and TIK lie nearly along the same latitude with a difference of 15° and 19° in magnetic and geographic longitudes respectively. Therefore, it was expected to record phase-coherent signals. On the contrary, anti-phase signals were monitored in instead. Hence, the phase shift between CHD and TIk arguably comes from the longitudinal tunneling of fast mode waves in the high latitude (Uozumi et al., 2004). Tokunaga

et al. (2007) studied the azimuthal wave number of the Pi-2s from these stations and found it to be about 3 which syncs with those obtained from high latitude regions as reported in previous works(e.g., Lester et al., 1983). In addition, the waveforms in CHD H and D components are noted to be slightly different with enhanced amplitudes. Thus, we suggest that the D and H fluctuations at the CHD station are initiated by a common source but with different generation mechanisms. Pi-2 waves in the CHD H component recording higher amplitudes are caused by FAC oscillations, i.e., field line resonance (Kim et al., 2005) while in the D perturbations are contributed by a combination of fast waves and FAC oscillations. This probably explains the shoot in Pi-2 amplitude compared to the TIK breaking the trend (refer to Figure 12) (Tokunaga et al., 2007).

Pi-2 pulsations detected in the sub-auroral zone lasted for about 10 minutes with similar H-bays arriving simultaneously with different wave profiles in D. The presence of group delays in the D components was also reported by other authors in their studies (e.g., Webster et al., 1989; Li et al., 1998; Hsu & McPherron, 2007). These Pi-2 beatings are manifestations of fast Alfven waves in the geomagnetic northward and FAC oscillations in the geomagnetic eastward (D) components. Subsequent increasing trends in amplitude from the equatorial to the auroral zone evidence wave power couplings or transfer into the L-shells away from the energy source (Saito, 1969; Rostoker & Samson, 1981). Fast mode waves driving Pi-2 magnetohydrodynamics waves in the lower latitudes require a longer time window to propagate through the plasmasphere. Hence causing smaller amplitudes in zones within $L \leq 2$. On the other hand, consistent and nearly monochromatic spectral patterns of Pi-2 pulsations in the sub-auroral zone were observed. It was proposed that early Pi-2s arriving on the northern components were triggered by fast-mode cavity resonance (PCR/PVR) as the generation mechanism rather than a periodic forcing by freely propagating fast-mode waves. It is also suggested that (PVR/PCR) cavity resonances are incapable of driving large amplitudes in the auroral zone (Takahashi et al., 2003). Interestingly WEP, BSV, and CAN detected the same Pi-2 pulses in both components. Furthermore, Similar H-bays and D-bays were observed with nearly the same amplitudes in H disturbances and exponentially increasing in D beats from WEP to CAN (refer to Figure 8 and 12). Therefore, global-mode oscillation must be associated with these components in the inner magnetosphere. A similar finding was also reported in their group studies on characteristics of low-latitude Pi-2 pulsations (Yumoto et al., 2001).

WEP and EWA in the low latitude region are located on opposite sides, where WEP is east of EWA with an exact time difference of 10 hours. Despite being along the same magnetic latitude, the Pi-2 pulsations recorded in them differ in both components. In EWA there was a clear wave polarisation while WEP reported none. This illustrates the latitudinal propagation of the Pi-2 wave property. The ellipticity in EWA as characterized in Figure 7 are direct consequence of surface waves generated by injection trajectories with distinct particle energies and flow diversions (Saka et al., 2010). On the other hand, the polarization of Pi-2 pulsations in PTK, ZYK, and MGD in the midlatitude zone was associated with phase modulation due to overhead currents (Uozumi et al., 2016b). There are two possible situations for this kind of polarisation occurring in the mid-latitude region; the transient response Pi-2 and PCR-Pi-2 (Allan et al., 1996). In the PCR model, the meridian of the fast-mode source coincides with the center meridian of the polarization pattern triggering the cavity while in the transient response model, the upward current of the Substorm Current Wedge is close to the center meridian (Uozumi et al., 2016a). Therefore, in PTK and MGD, the center meridian was close to 210° which is also coherent with the Lester et al. (1983) findings. The observation in the auroral zone demonstrates a modulation of Pi-2 pulsations scaling with an increase in L- value maximum at KTN and minimum in KOT. The influence of external effects such as local sea currents heavily attenuated the signal arriving at the ONW station in the D component. Therefore, the wave power in the H-component was stable and resistant to local effects while those in D were susceptible implying received Pi-2s are less energetic. The Pi-2 pulsation modulation by the sea currents due to ONW's proximity to the sea shows the need

to factor external influences in Pi-2 analysis aside from noise. This observation portrays the Pi-2 reception powers and local influences at D components compared to H counterparts making the wavelet technique a useful tool in analysis.

5 Conclusion

In summary, the ground Pi-2 Pulsations detected in the 210° MM network consisted of various irregular modal components indicating the tunneling of shear and fast Alfven waves, field line resonances, and finally plasmaspheric resonances. The influences of local effects such as sea currents are also emphasized affecting the reception of Pi-2 signals in some monitors in the CPMN network. Thus, highlighting the consequence of considering local environmental effects in data analysis. During the onset of the substorm expansion, the near-Earth magnetotail suddenly reconfigured to a dipole state from its original physical state of stretched configuration. The change in the magnetosphere configuration is instigated by the formation of the substorm current wedge (SCW), when the cross-tail current gets short-circuited to the auroral ionosphere via field-aligned currents, due to the disruption of the tail current. Pi-2 pulsations are regarded as the manifestation of the sudden change in the state of the magnetosphere during a substorm, which can be monitored at different radial distances from the Earth's surface. In conclusion, this study provides valuable insights into the features of Pi-2 pulsations in the sub-auroral to the auroral zone. Their latitudinal and longitudinal propagation and initiation mechanisms. Finally, their variations across different magnetic latitudes along narrow meridians. The association of Pi-2 pulsations with substorms is an important proxy for understanding the coupling process between the magnetosphere-ionosphere coupling and the complex electrodynamic processes in the magnetosphere. The successful application of the wavelet analytic detection technique of Pi-2 pulsation in the current study makes it a valuable tool for future research in the magnetospheric community. Mapping global simulations with ground observations to complement limited space observations would provide a comprehensive understanding of mixing systems in the ionospheric and magnetosphere.

Acknowledgments

This work was collaboratively supported by the Scientific Committee on Solar-Terrestrial Physics (SCOSTEP) SVS program and the International Research Center for Space and Planetary Environmental Science (i-SPES or ICSWSE) in Kyushu University under PI Prof.Akimasa Yoshikawa. The data were provided by the principal investigator of the MAGDAS/CPMN project `http://magdas.serc.kyushu-u.ac.jp/`. I extend my humble gratitude to the SCOSTEP team and i-SPES research group for their joint support for my 3 months visit and research in Japan. I acknowledge the generosity and well-being provided by the Japanese research colleagues for my happy stay and Japanese experience. I also appreciate the involuntary support provided by Egypt Japan University of Science and Technology in facilitating my visit to and from Japan through Prof. Ayman Mahrous. The author gives much appreciation to the MAGDAS team for their effort and dedication in maintaining and making MAGDAS/CPMN magnetic data available for public use.

References

Allan, W., Menk, F., Fraser, B., Li, Y., & White, S. (1996). Are low-latitude pi2 pulsations cavity/waveguide modes? *Geophysical research letters*, *23*(7), 765–768.

Balasis, G., Aminalragia-Giamini, S., Papadimitriou, C., Daglis, I. A., Anastasiadis, A., & Haagmans, R. (2019). A machine learning approach for automated ulf wave recognition. *Journal of Space Weather and Space Climate*, *9*, A13.

Baumjohann, W., & Glaßmeier, K.-H. (1984). The transient response mechanism and pi2 pulsations at substorm onset—review and outlook. *Planetary and Space Science*, *32*(11), 1361–1370.

Clauer, C. R., & McPherron, R. L. (1974). Mapping the local time-universal time development of magnetospheric substorms using mid-latitude magnetic observations. *Journal of Geophysical Research*, *79*(19), 2811–2820.

Cohen, A., Daubechies, I., & Feauveau, J.-C. (1992). Biorthogonal bases of compactly supported wavelets. *Communications on pure and applied mathematics*, *45*(5), 485–560.

Daubechies, I. (1988). Orthonormal bases of compactly supported wavelets. *Communications on Pure and Applied Mathematics*, *41*(7), 909-996. doi: https://doi.org/10.1002/cpa.3160410705

Daubechies, I. (1992). *Ten lectures on wavelets*. SIAM.

Forsyth, C., Rae, I., Coxon, J., Freeman, M., Jackman, C., Gjerloev, J., & Fazakerley, A. (2015). A new technique for determining substorm onsets and phases from indices of the electrojet (sophie). *Journal of Geophysical Research: Space Physics*, *120*(12), 10–592.

Fukunishi, H. (1975). Polarization changes of geomagnetic pi 2 pulsations associated with the plasmapause. *Journal of Geophysical Research (1896-1977)*, *80*(1), 98-110. doi: https://doi.org/10.1029/JA080i001p00098

Hafez, A. G., Ghamry, E., Yayama, H., & Yumoto, K. (2012). A wavelet spectral analysis technique for automatic detection of geomagnetic sudden commencements. *IEEE Transactions on Geoscience and Remote Sensing*, *50*(11), 4503-4512. doi: 10.1109/TGRS.2012.2192279

Hafez, A. G., Khan, M. T. A., & Kohda, T. (2010). Clear p-wave arrival of weak events and automatic onset determination using wavelet filter banks. *Digital Signal Processing*, *20*(3), 715-723. doi: https://doi.org/10.1016/j.dsp.2009.10.002

Hsu, T.-S., McPherron, R., Angelopoulos, V., Ge, Y., Zhang, H., Russell, C., ... Kissinger, J. (2012). A statistical analysis of the association between fast plasma flows and pi2 pulsations. *Journal of Geophysical Research: Space Physics*, *117*(A11).

Hsu, T.-S., & McPherron, R. L. (2007). A statistical study of the relation of pi 2 and plasma flows in the tail. *Journal of Geophysical Research: Space Physics*, *112*(A5). doi: https://doi.org/10.1029/2006JA011782

Jach, A., Kokoszka, P., Sojka, J., & Zhu, L. (2006). Wavelet-based index of magnetic storm activity. *Journal of Geophysical Research: Space Physics*, *111*(A9). doi: https://doi.org/10.1029/2006JA011635

Keiling, A., Marghitu, O., Vogt, J., Amm, O., Bunescu, C., Constantinescu, V., ... Sorbalo, E. (2014a). Magnetosphere-ionosphere coupling of global pi2 pulsations. *Journal of Geophysical Research: Space Physics*, *119*(4), 2717-2739. doi: https://doi.org/10.1002/2013JA019085

Keiling, A., Marghitu, O., Vogt, J., Amm, O., Bunescu, C., Constantinescu, V., ... others (2014b). Magnetosphere-ionosphere coupling of global pi2 pulsations. *Journal of Geophysical Research: Space Physics*, *119*(4), 2717–2739.

Keiling, A., Mozer, F., Reme, H., Dandouras, I., Lucek, E., Fujimoto, M., ... Reeves, G. (2008). Periodic traveling compression regions during quiet geomagnetic conditions and their association with ground pi2. In *Annales geophysicae* (Vol. 26, pp. 3341–3354).

Keiling, A., & Takahashi, K. (2011). Review of pi2 models. *Space Science Reviews*, *161*, 63–148.

Kepko, L., Kivelson, M., & Yumoto, K. (2001). Flow bursts, braking, and pi2 pulsations. *Journal of Geophysical Research: Space Physics*, *106*(A2), 1903–1915.

Kim, K.-H., Lee, D.-H., Denton, R.-E., Takahashi, K., Goldstein, J., Moon, Y.-J., ... Keiling, A. (2005). Pi2 pulsations in a small and strongly asymmetric

plasmasphere. *Journal of Geophysical Research: Space Physics*, *110*(A10).

Kumar, P., & Foufoula-Georgiou, E. (1997). Wavelet analysis for geophysical applications. *Reviews of Geophysics*, *35*(4), 385-412. doi: https://doi.org/10.1029/97RG00427

Lee, D.-H., & Lysak, R. L. (1999). Mhd waves in a three-dimensional dipolar magnetic field: A search for pi2 pulsations. *Journal of Geophysical Research: Space Physics*, *104*(A12), 28691–28699.

Lester, M., Hughes, J. W., & Singer, H. J. (1983). Polarization patterns of pi 2 magnetic pulsations and the substorm current wedge. *Journal of Geophysical Research: Space Physics*, *88*(A10), 7958–7966.

Li, Y., Fraser, B. J., Menk, F. W., Webster, D. J., & Yumoto, K. (1998). Properties and sources of low and very low latitude pi2 pulsations. *Journal of Geophysical Research: Space Physics*, *103*(A2), 2343-2358. doi: https://doi.org/10.1029/97JA02921

Lin, C., Lee, L., & Sun, Y. (1991). Observations of pi 2 pulsations at a very low latitude (l= 1.06) station and magnetospheric cavity resonances. *Journal of Geophysical Research: Space Physics*, *96*(A12), 21105–21113.

Mallat, S. (2009). *A wavelet tour of signal processing, chapters 1 and 12.* Academic Press Chicago.

Mallat, S. G. (1989). A theory for multiresolution signal decomposition: the wavelet representation. *IEEE Transactions on pattern analysis and machine intelligence*, *11*(7), 674–693. doi: 10.1109/34.192463

Omondi, S., Yoshikawa, A., Zahra, W. K., Fathy, I., & Mahrous, A. (2023a). Alex magnetometer and telluric station in egypt: First results on pulsation analysis. *Advances in Space Research*, *72*(3), 711-725. (Space and Geophysical Observations and Recent Results related to the African Continent) doi: https://doi.org/10.1016/j.asr.2022.09.014

Omondi, S., Yoshikawa, A., Zahra, W. K., Fathy, I., & Mahrous, A. (2023b). Automatic detection of auroral pc5 geomagnetic pulsation using machine learning approach guided with discrete wavelet transform. *Advances in Space Research*, *72*(3), 866-883. doi: https://doi.org/10.1016/j.asr.2022.06.063

Romero, L., Hypolite, D., & McWilliams, J. C. (2020). Submesoscale current effects on surface waves. *Ocean Modelling*, *153*, 101662.

Rostoker, G., & Samson, J. C. (1981). Polarization characteristics of pi 2 pulsations and implications for their source mechanisms: Location of source regions with respect to the auroral electrojets. *Planetary and Space Science*, *29*(2), 225-247. doi: https://doi.org/10.1016/0032-0633(81)90036-2

Saito, T. (1969). Geomagnetic pulsations. *Space Science Reviews*, *10*(3), 319–412.

Saka, O., Hayashi, K., & Thomsen, M. F. (2010). First 10 min intervals of pi2 onset at geosynchronous altitudes during the expansion of energetic ion regions in the nighttime sector. *Journal of Atmospheric and Solar-Terrestrial Physics*, *72*, 1100-1109.

Sakurai, T., & Saito, T. (1976). Magnetic pulsation pi2 and substorm onset. *Planetary and Space Science*, *24*(6), 573–575.

Samson, J. (1982). Pi 2 pulsations: High latitude results. *Planetary and Space Science*, *30*(12), 1239-1247. doi: https://doi.org/10.1016/0032-0633(82)90097-6

Singer, H. J., Hughes, W. J., Fougere, P. F., & Knecht, D. J. (1983). The localization of pi 2 pulsations: Ground-satellite observations. *Journal of Geophysical Research: Space Physics*, *88*(A9), 7029-7036. doi: https://doi.org/10.1029/JA088iA09p07029

Sutcliffe, P. R., & Yumoto, K. (1989). Dayside pi 2 pulsations at low latitudes. *Geophysical research letters*, *16*(8), 887–890.

Sutcliffe, P. R., & Yumoto, K. (1991). On the cavity mode nature of low-latitude pi 2 pulsations. *Journal of Geophysical Research: Space Physics*, *96*(A2), 1543–1551.

Takahashi, K., Hughes, W., Anderson, R., & Solovyev, S. (1999). Crres satellite observations associated with low-latitude pi2 pulsations. *Journal of Geophysical Research: Space Physics*, *104*(A8), 17431–17440.

Takahashi, K., Lee, D.-H., Nosé, M., Anderson, R. R., & Hughes, W. J. (2003). Crres electric field study of the radial mode structure of pi2 pulsations. *Journal of Geophysical Research: Space Physics*, *108*(A5).

Takahashi, K., Ohtani, S.-i., & Anderson, B. J. (1995). Statistical analysis of pi 2 pulsations observed by the ampte cce spacecraft in the inner magnetosphere. *Journal of Geophysical Research: Space Physics*, *100*(A11), 21929–21941.

Teramoto, M., Nosé, M., & Sutcliffe, P. (2008). Statistical analysis of pi2 pulsations inside and outside the plasmasphere observed by the polar orbiting de-1 satellite. *Journal of Geophysical Research: Space Physics*, *113*(A7).

Tokunaga, T., Kohta, H., Yoshikawa, A., Uozumi, T., & Yumoto, K. (2007). Global features of pi 2 pulsations obtained by independent component analysis. *Geophysical Research Letters*, *34*(14). doi: https://doi.org/10.1029/2007GL030174

Uozumi, T., Abe, S., Kitamura, K., Tokunaga, T., Yoshikawa, A., Kawano, H., ... Yumoto, K. (2009). Propagation characteristics of pi 2 pulsations observed at high- and low-latitude magdas/cpmn stations: A statistical study. *Journal of Geophysical Research: Space Physics*, *114*(A11). doi: https://doi.org/10.1029/2009JA014163

Uozumi, T., Yoshikawa, A., Ohtani, S., Imajo, S., Baishev, D., Moiseev, A., & Yumoto, K. (2016b). Initial deflection of middle-latitude pi2 pulsations in the premidnight sector: Remote detection of oscillatory upward field-aligned current at substorm onset. *Journal of Geophysical Research: Space Physics*, *121*(7), 6324–6340.

Uozumi, T., Yoshikawa, A., Ohtani, S., Imajo, S., Baishev, D. G., Moiseev, A. V., & Yumoto, K. (2016a). Initial deflection of middle-latitude pi2 pulsations in the premidnight sector: Remote detection of oscillatory upward field-aligned current at substorm onset. *Journal of Geophysical Research: Space Physics*, *121*(7), 6324-6340. doi: https://doi.org/10.1002/2015JA021698

Uozumi, T., Yumoto, K., Kawano, H., Yoshikawa, A., Ohtani, S., Olson, J., ... others (2004). Propagation characteristics of pi 2 magnetic pulsations observed at ground high latitudes. *Journal of Geophysical Research: Space Physics*, *109*(A8).

Uozumi, T., Yumoto, K., Kawano, H., Yoshikawa, A., Olson, J., Solovyev, S., & Vershinin, E. (2000). Characteristics of energy transfer of pi 2 magnetic pulsations: Latitudinal dependence. *Geophysical Research Letters*, *27*(11), 1619–1622.

Uozumi, T., Yumoto, K., Tokunaga, T., Solovyev, S. I., Shevtsov, B. M., Marshall, R., ... Itonaga, M. (2011). Akr modulation and global pi2 oscillation. *Journal of Geophysical Research: Space Physics*, *116*(A6). doi: https://doi.org/10.1029/2010JA016042

Vetterli, M. (1986). Filter banks allowing perfect reconstruction. *Signal processing*, *10*(3), 219–244.

Webster, D. J., Samson, J. C., & Rostoker, G. (1989). Eastward propagation of transient field-aligned currents and pi 2 pulsations at auroral latitudes. *Journal of Geophysical Research: Space Physics*, *94*(A4), 3619-3630. doi: https://doi.org/10.1029/JA094iA04p03619

Xu, Z., Zhu, L., Sojka, J., Kokoszka, P., & Jach, A. (2008). An assessment study of the wavelet-based index of magnetic storm activity (wisa) and its comparison to the dst index. *Journal of Atmospheric and Solar-Terrestrial Physics*, *70*(11), 1579-1588. doi: https://doi.org/10.1016/j.jastp.2008.05.007

yang Zeng, X., & guang Wang, S. (2013). Bark-wavelet analysis and hilbert–huang transform for underwater target recognition. *Defence Technology*, *9*(2), 115-

120. doi: https://doi.org/10.1016/j.dt.2012.09.001

Yeoman, T., & Orr, D. (1989). Phase and spectral power of mid-latitude pi2 pulsations: Evidence for a plasmaspheric cavity resonance. *Planetary and space science*, *37*(11), 1367–1383.

Yumoto, K. (1990). Evidences of magnetospheric cavity pi2 waves. *Journal of geomagnetism and geoelectricity*, *42*(11), 1281–1290.

Yumoto, K., group, C., et al. (2001). Characteristics of pi 2 magnetic pulsations observed at the cpmn stations a review of the step results. *Earth, planets and space*, *53*(10), 981–992.

M_2.png.

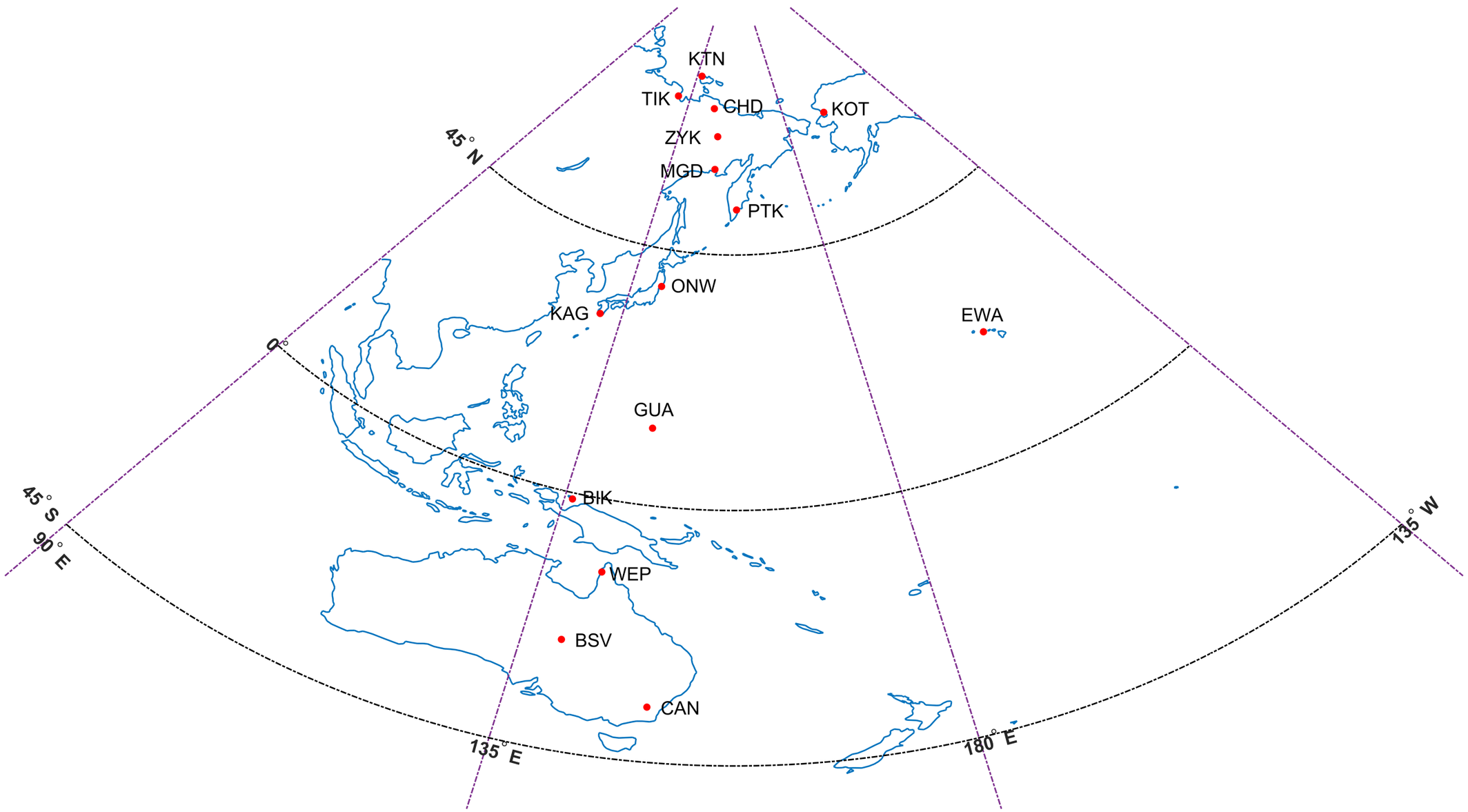
KTN
TIK
CHD
KOT
ZYK
MGD
PTK
ONW
KAG
EWA
GUA
BIK
WEP
BSV
CAN
45° N
0°
45° S
90° E
135° E
180° E
135° W

Pi-2.jpg.

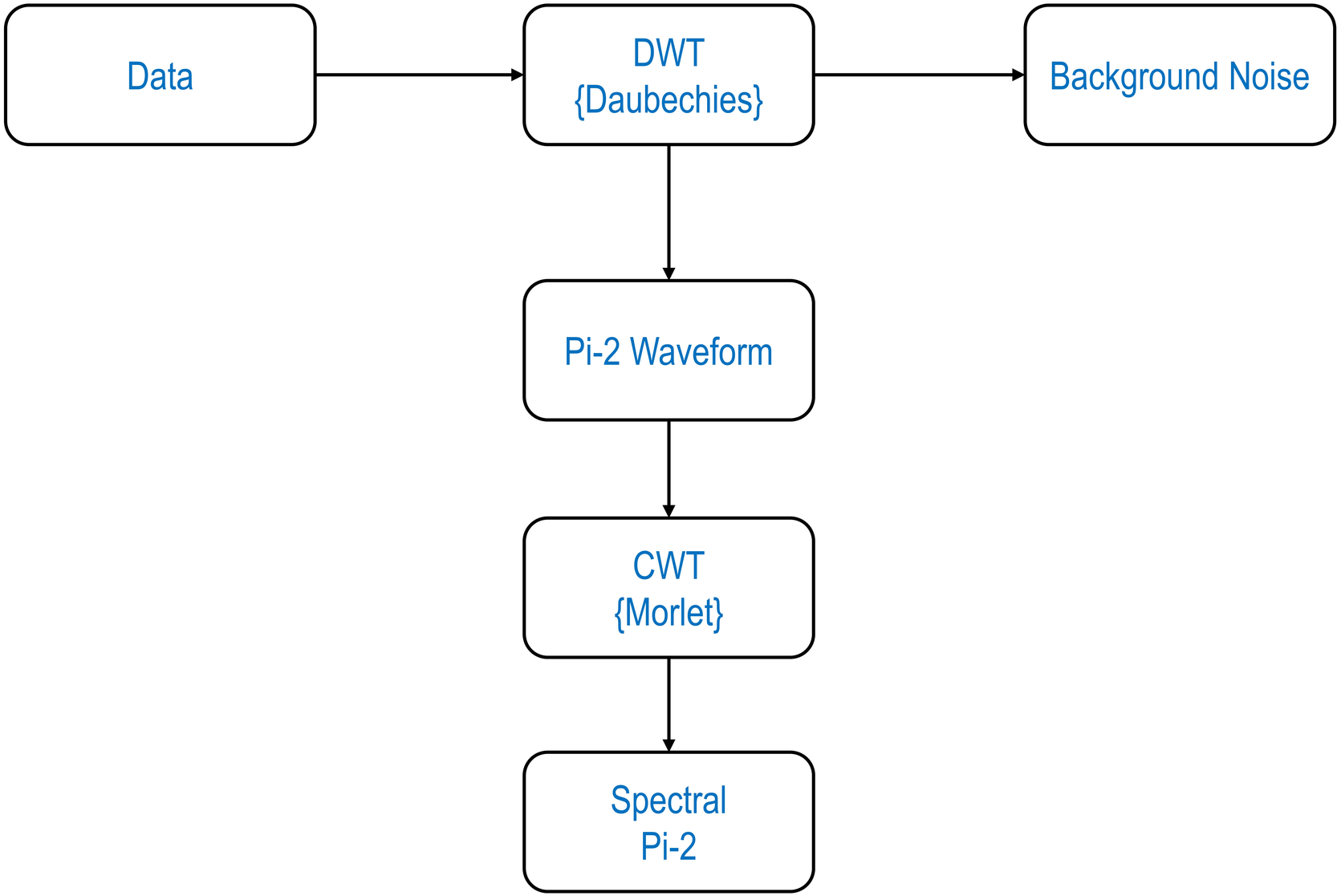
Data
DWT
{Daubechies}
Background Noise
Pi-2 Waveform
CWT
{Morlet}
Spectral
Pi-2

NS.png.

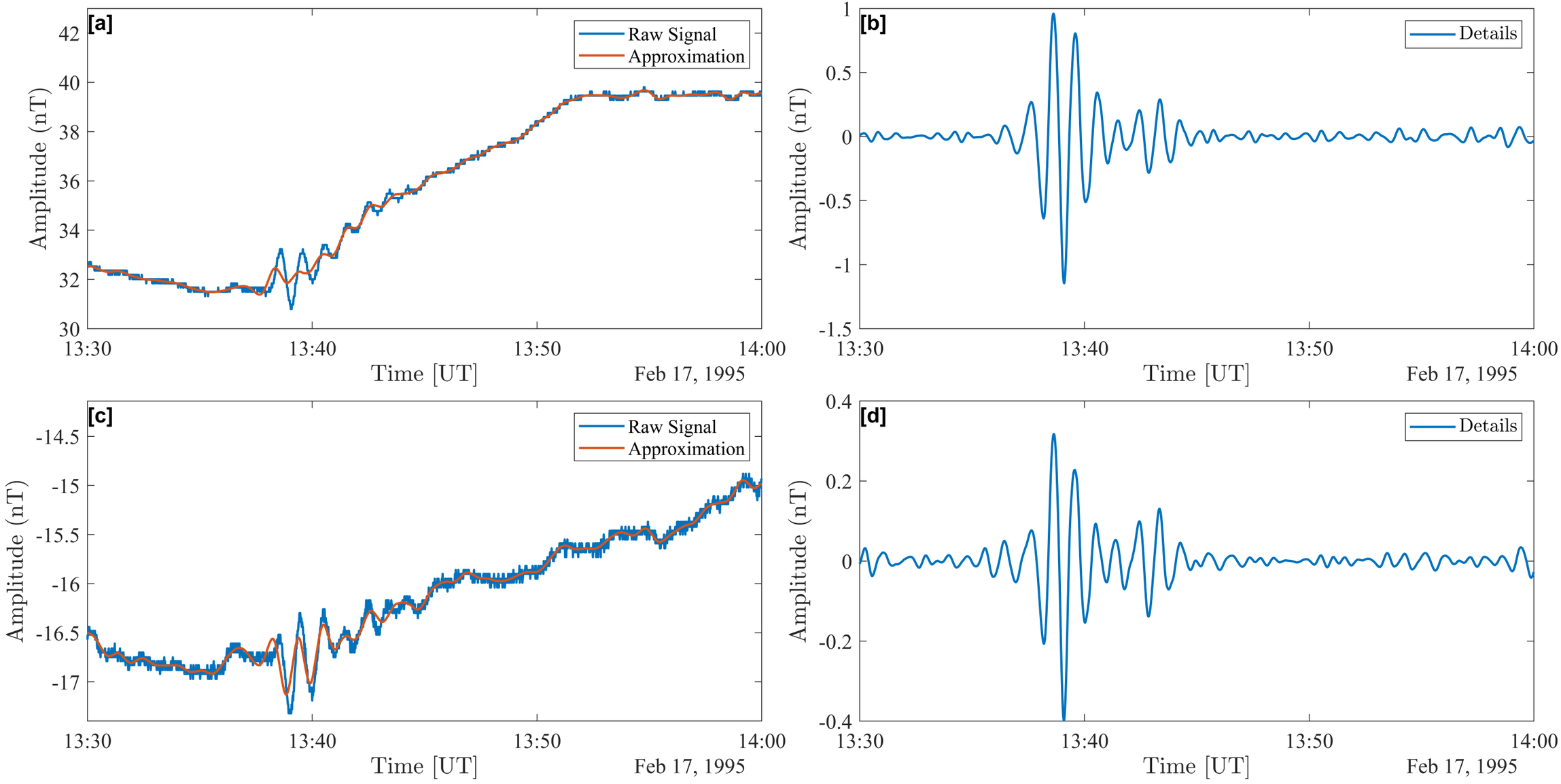
[a]
Raw Signal
Approximation
Amplitude (nT)
42
40
38
36
34
32
30
13:30
13:40
13:50
14:00
Time [UT]
Feb 17, 1995
[b]
Details
Amplitude (nT)
1
0.5
0
-0.5
-1
-1.5
13:30
13:40
13:50
14:00
Time [UT]
Feb 17, 1995
[c]
Raw Signal
Approximation
Amplitude (nT)
-14.5
-15
-15.5
-16
-16.5
-17
13:30
13:40
13:50
14:00
Time [UT]
Feb 17, 1995
[d]
Details
Amplitude (nT)
0.4
0.2
0
-0.2
-0.4
13:30
13:40
13:50
14:00
Time [UT]
Feb 17, 1995

mid_MGD1.png.

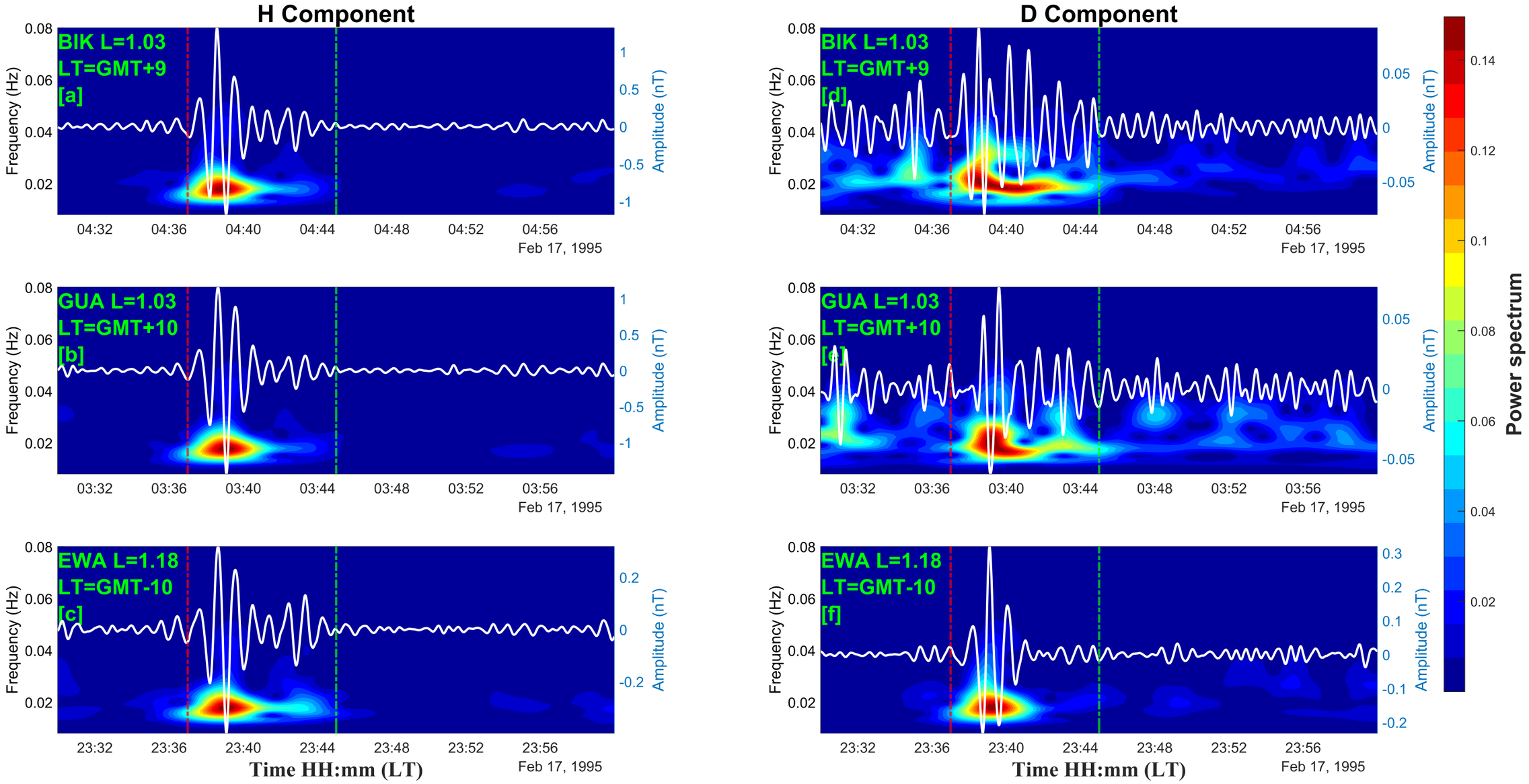
H Component
D Component
BIK L=1.03
LT=GMT+9
[a]
[d]
GUA L=1.03
LT=GMT+10
[b]
[e]
EWA L=1.18
LT=GMT-10
[c]
[f]
Frequency (Hz)
Amplitude (nT)
Power spectrum
Time HH:mm (LT)
Feb 17, 1995

mid_MGD2.png.

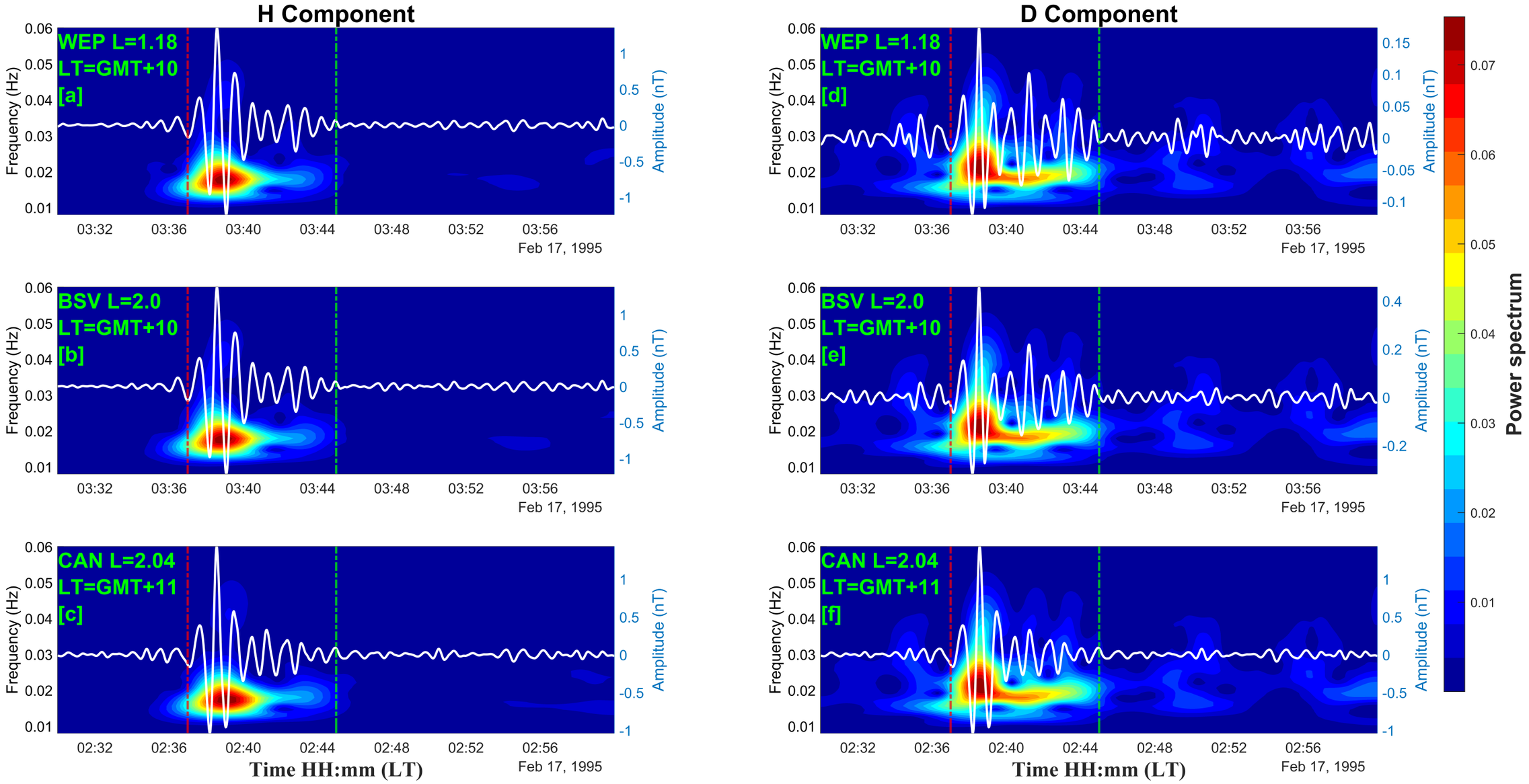
H Component
D Component
WEP L=1.18
LT=GMT+10
[a]
[d]
BSV L=2.0
LT=GMT+10
[b]
[e]
CAN L=2.04
LT=GMT+11
[c]
[f]
Frequency (Hz)
Amplitude (nT)
Power spectrum
Time HH:mm (LT)
Feb 17, 1995

mid_MGD3.png.

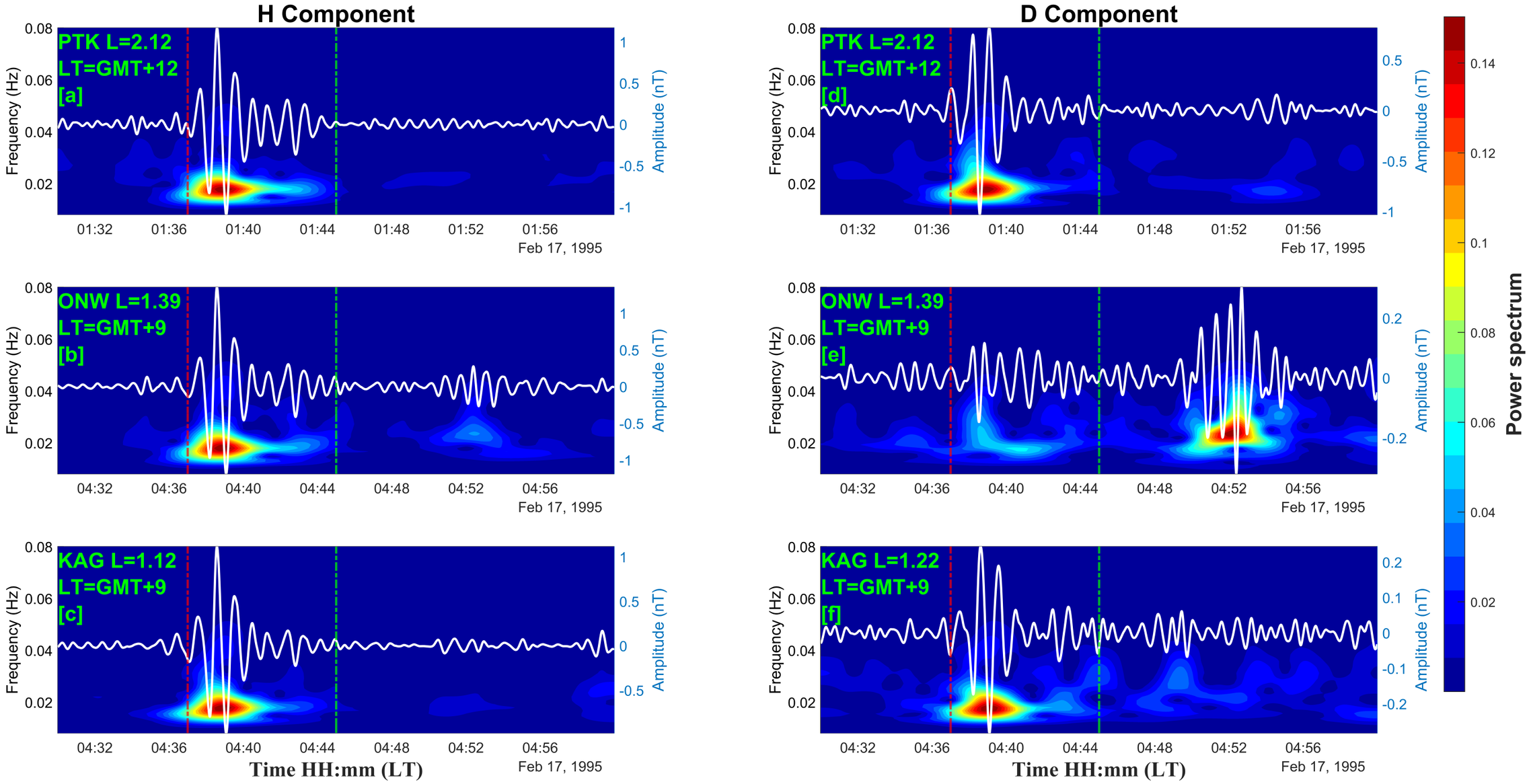
H Component
D Component
PTK L=2.12
LT=GMT+12
[a]
[d]
ONW L=1.39
LT=GMT+9
[b]
[e]
KAG L=1.12
LT=GMT+9
[c]
KAG L=1.22
LT=GMT+9
[f]
Frequency (Hz)
Amplitude (nT)
Power spectrum
Time HH:mm (LT)
Feb 17, 1995

P1.png.

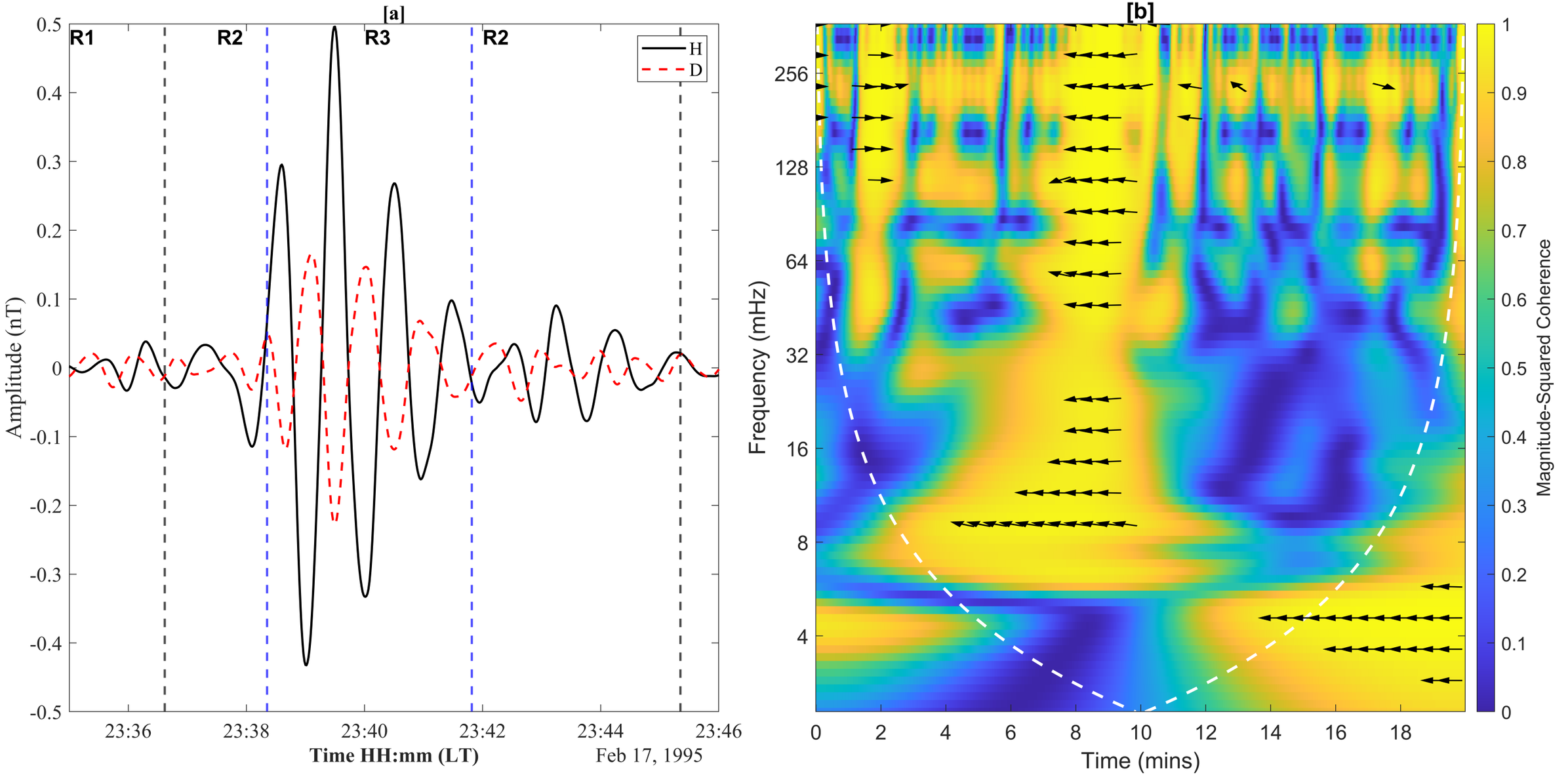
[a]
R1
R2
R3
R2
H
D
Amplitude (nT)
0.5
0.4
0.3
0.2
0.1
0
-0.1
-0.2
-0.3
-0.4
-0.5
23:36
23:38
23:40
23:42
23:44
23:46
Time HH:mm (LT)
Feb 17, 1995
[b]
Frequency (mHz)
256
128
64
32
16
8
4
0
2
4
6
8
10
12
14
16
18
Time (mins)
Magnitude-Squared Coherence
1
0.9
0.8
0.7
0.6
0.5
0.4
0.3
0.2
0.1
0

MaGd_L.png.

(a)

PTK
ONW
KAG
EWA
GUA
BIK
WEP
BSV
CAN

46.17°
31.15°
24.37°
21.63°
5.61°
−9.73°
−21.93°
−36.10°
−45.72°

Magnetic Latitude (°)

17 13:30 17 13:35 17 13:40 17 13:45 17 13:50 17 13:55 17 14:00

Time HH:mm (UT)

(b)

46.17°
31.15°
24.37°
21.63°
5.61°
−9.73°
−21.93°
−36.10°
−45.72°

Magnetic Latitude (°)

17 13:30 17 13:35 17 13:40 17 13:45 17 13:50 17 13:55 17 14:00

Time HH:mm (UT)

HN2.png.

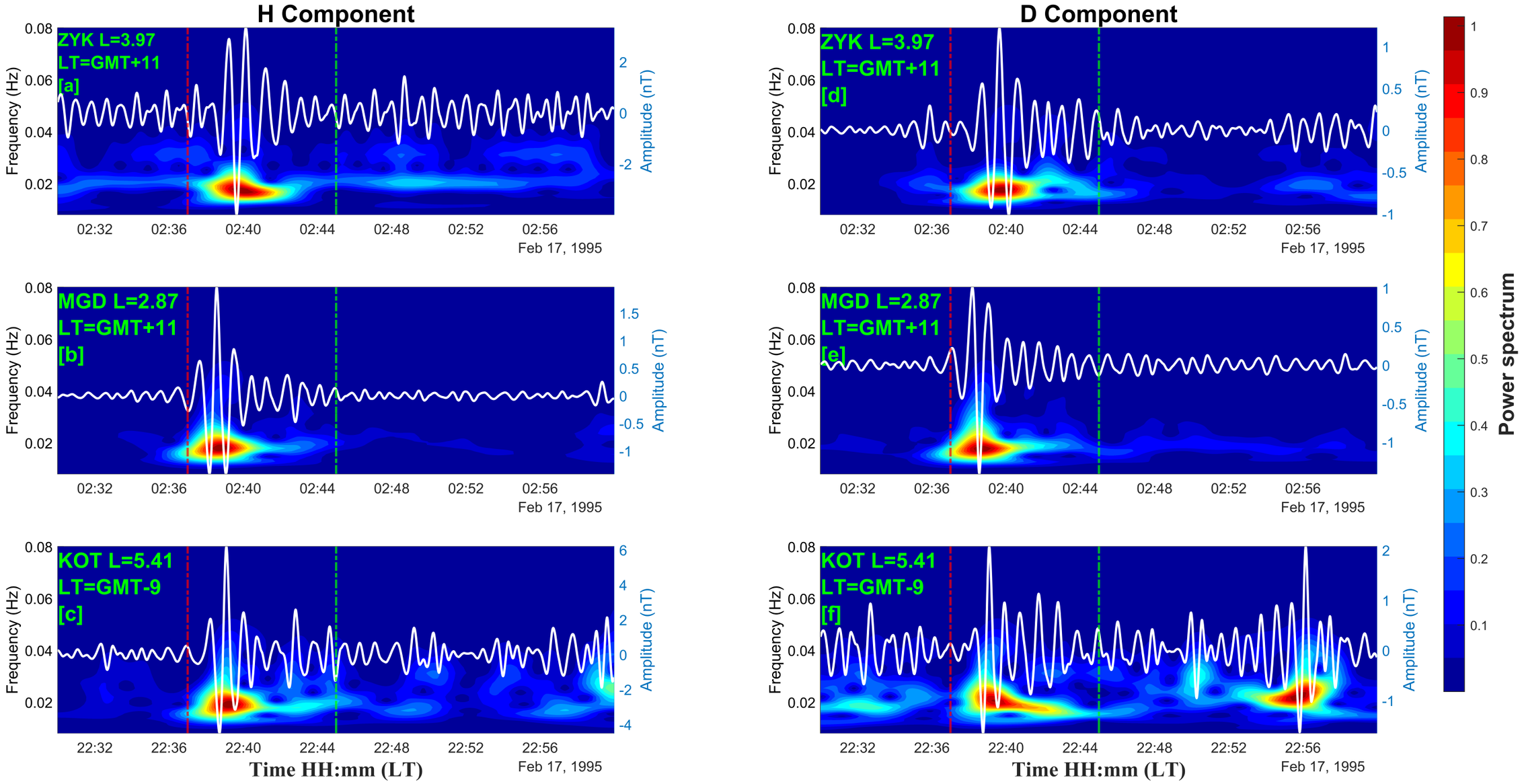
H Component
D Component
ZYK L=3.97
LT=GMT+11
[a]
[d]
MGD L=2.87
LT=GMT+11
[b]
[e]
KOT L=5.41
LT=GMT-9
[c]
[f]
Frequency (Hz)
Amplitude (nT)
Power spectrum
Time HH:mm (LT)
Feb 17, 1995

HN1.png.

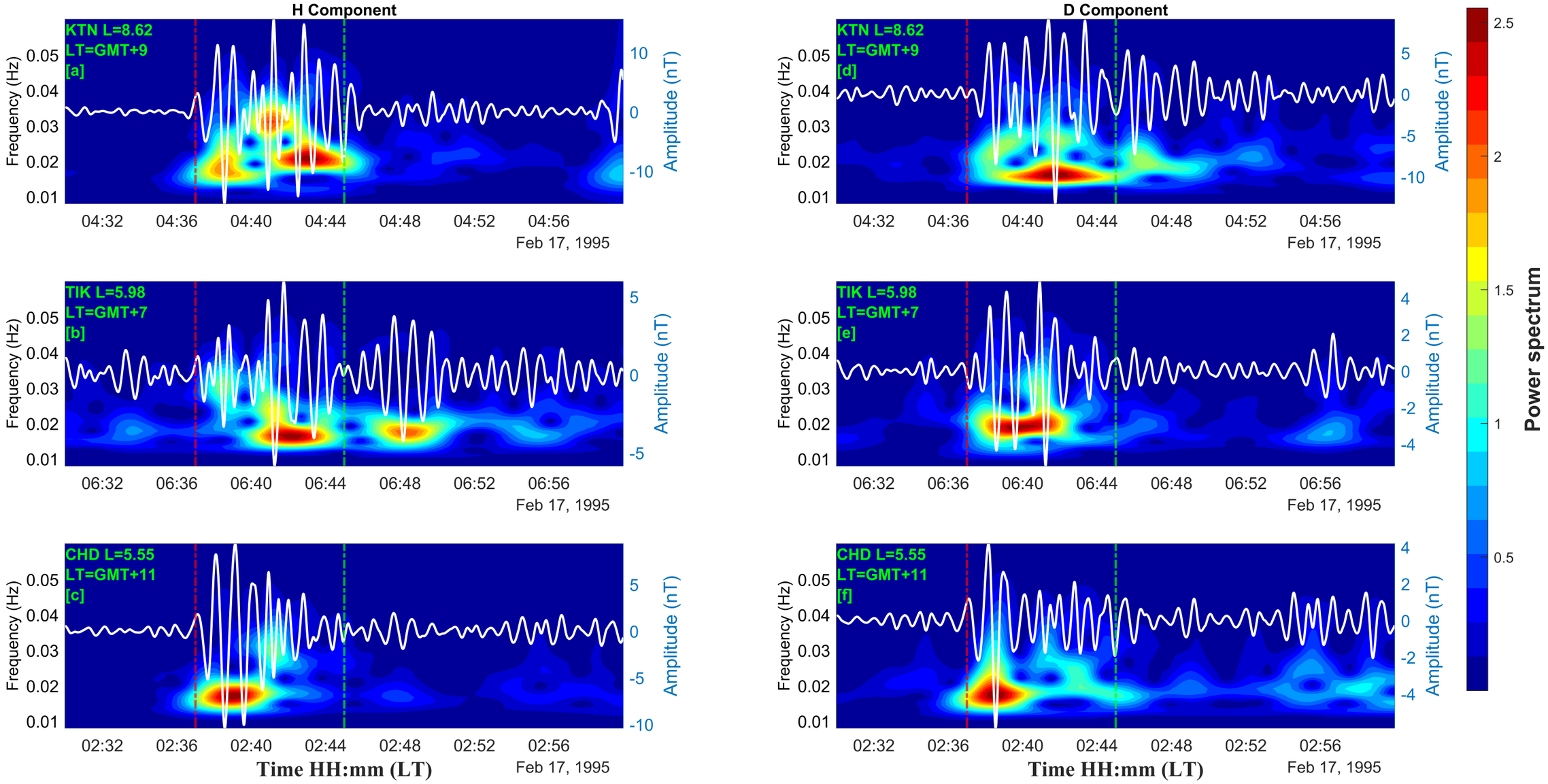
H Component
D Component
KTN L=8.62
LT=GMT+9
[a]
[d]
TIK L=5.98
LT=GMT+7
[b]
[e]
CHD L=5.55
LT=GMT+11
[c]
[f]
Frequency (Hz)
Amplitude (nT)
Power spectrum
Time HH:mm (LT)
Feb 17, 1995

MaGd_H.png.

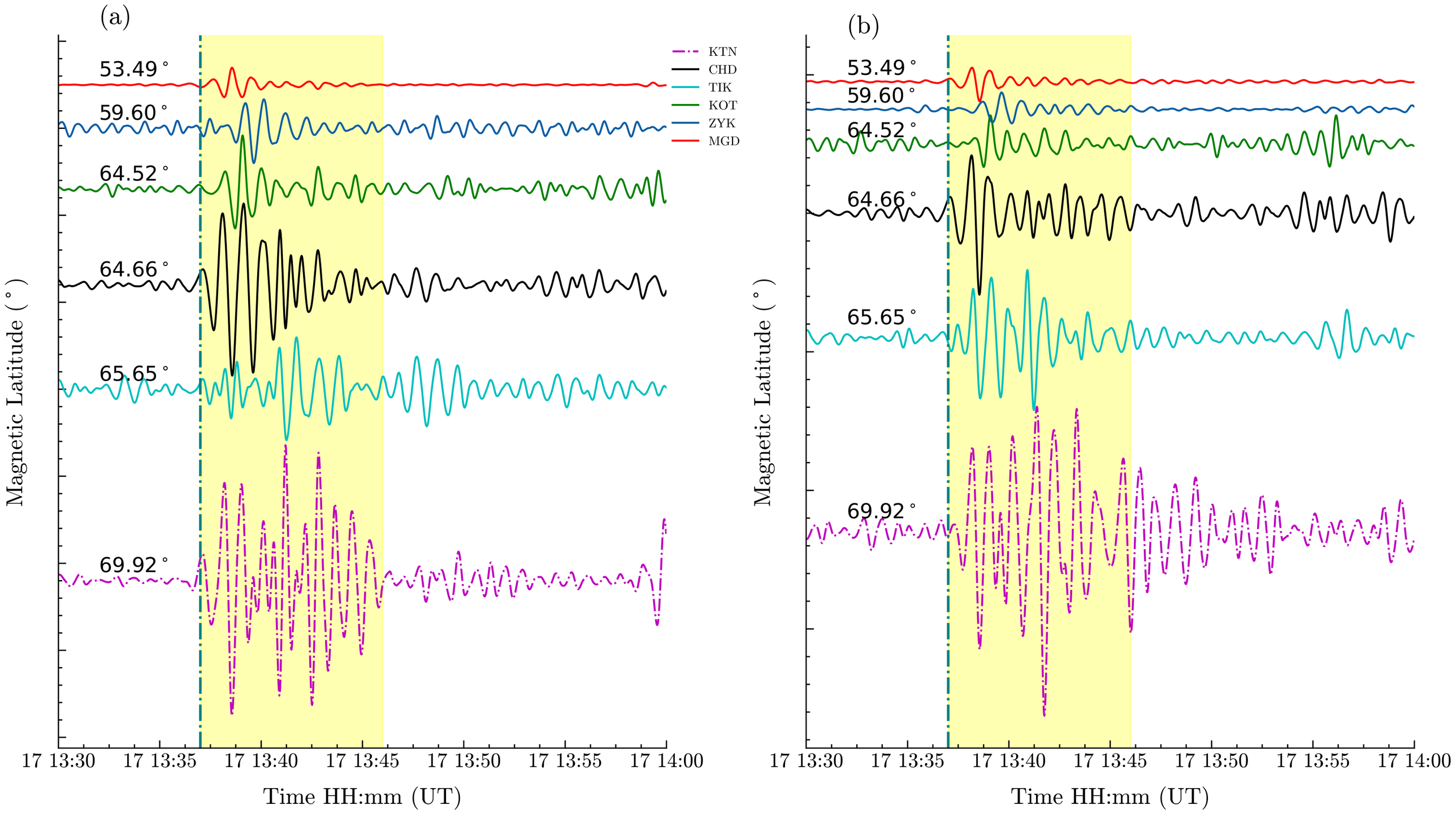
(a)
(b)
KTN
CHD
TIK
KOT
ZYK
MGD
53.49°
59.60°
64.52°
64.66°
65.65°
69.92°
Magnetic Latitude (°)
17 13:30
17 13:35
17 13:40
17 13:45
17 13:50
17 13:55
17 14:00
Time HH:mm (UT)

MaGd.png.

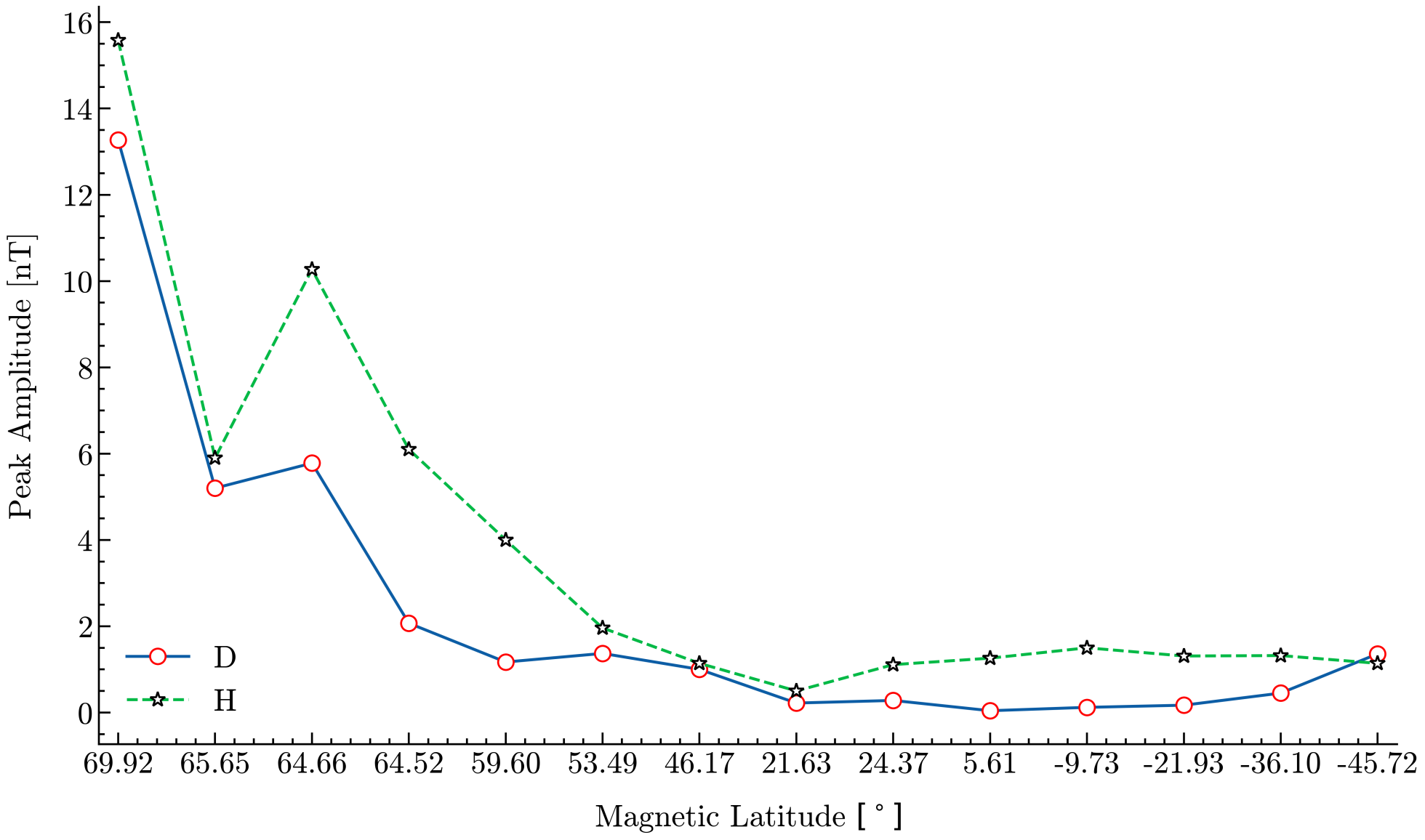
Peak Amplitude [nT]
16
14
12
10
8
6
4
2
0
D
H
69.92
65.65
64.66
64.52
59.60
53.49
46.17
21.63
24.37
5.61
-9.73
-21.93
-36.10
-45.72
Magnetic Latitude [°]

Wavelet Analysis for Automatic Detection of Pi-2 Pulsations during Substorm Onset Along the 210° Magnetic Meridian

Stephen Omondi[1,2], Akimasa Yoshikawa[2,3], T. Uozumi[2,3], Yuki Obana[2,3], Moe Hayashi [2,3], Ayman Mahrous[1,4]

[1]Department of Space Environment, Institute of Basic and Applied Sciences, Egypt-Japan University of Science and Technology (E-JUST), New Borg El-Arab City, Alexandria 21934, Egypt
[2]International Center for Space Weather Science and Education, Kyushu University, Fukuoka, Japan
[3]Department of Earth and Planetary Science, Kyushu University, Fukuoka, Japan
[4]Department of Physics, Faculty of Science, Helwan University, Helwan, Cairo, Egypt

Key Points:

- Wavelet automatic detection performed excellently well in Pi-2 detection from auroral to sub-auroral zone.
- Manifestations of latitudinal and longitudinal Pi-2 undulations illustrated by the ellipticities and group delays.
- Influence of dominance of external effect such as sea currents were uncovered resulting in Pi-2s heavily attenuated.

Corresponding author: Stephen Omondi, stephen.owino.omondi@outlook.com

Abstract

Ground Pi-2 pulsations comprise superpositions of various modal components of shear and fast Alfven waves, field line resonance, and plasmaspheric resonances. These complex waveforms, hard to resolve with Fourier transforms are successfully characterized by wavelet techniques. Wavelet detection employs decomposition and reconstruction modes to characterize time-frequency components. Hence, suitable for the examination of the locality and complexity of natural signal patterns. The current study presents the automatic detection of Pi-2 pulsations using Daubechies and Morlet wavelet transforms. In the study, distinct Pi-2 events from CPMN stations along 210° magnetic meridian were detected. Global Pi-2 pulsations with harmonious H oscillations and discrete D bays in the sub-aurora zone suggest a common source with diverse tunneling paths. Scalograms of Pi-2 undulations of the frequency band of 6.7-22 mHz were observed despite different kinds of Pi-2s. Auroral Pi-2s were highly localized in local time with clear H and D bays, implying magnetospheric-ionospheric current couplings. Latitudinal and longitudinal Pi-2 propagations are exemplified by 180° phase-shift (polarization) in EWA and group delay in the mid-latitudes of the northern hemisphere. Overall, Pi-2 wave power from high to low latitudes declined with peak amplitudes of 15 nT to less than 1 nT, respectively. Finally, external influences from sea currents causing signal attenuation due to the station's proximity to the sea were also identified. To conclude, the accuracy and efficiency of wavelet analysis with no computation hassle render it a valuable tool for the study of space events in the magnetospheric community.

1 Introduction

Pi-2 pulsations are transient, irregular geomagnetic oscillations with periods ranging from 40 s to 150 s (Singer et al., 1983). These magnetohydrodynamic waves are usually observed at the onset of substorm expansions and auroral breakups (Sakurai & Saito, 1976). One remarkable property of Pi-2 undulations is their extensive spatial distributions. They span from local magnetic time (MLT) and/or invariable latitudes to global events covering many hours of MLT extending from low to high latitudes. This spatial variability is believed to reflect different Pi-2s generation mechanisms (e.g., Keiling & Takahashi, 2011). Studies based on observations have illustrated that Pi-2 pulsations monitored on the ground consist of superpositions of different components (Yumoto et al., 2001). At low latitudes, the Pi-2 beats observed at different latitudes and longitudes occur with a common waveform and frequency(Sutcliffe & Yumoto, 1991). Recent studies suggest these low-latitude Pi-2 pulsations are generated by cavity resonances excited by earthward-propagating fast mode waves launched at substorm commencement(Yumoto, 1990; Takahashi et al., 1995; Allan et al., 1996; Kepko et al., 2001; Hsu et al., 2012). In contrast, mid-latitude Pi-2 pulsations are believed to originate from the disturbance of cross-tail current associated with Alfven waves carrying field-aligned currents, which play a role in the substorm current wedge establishment (Sakurai & Saito, 1976).

Statistical studies on space and ground-based Pi-2 pulsations indicated that regions inside the inner magnetosphere (L = 2 to 5) 3 hours past their local midnight are dominated by poloidal components such as compressional (Bz) and radial (Bx). These components correspond to fast mode waves polarized in the direction of their Meridian (Baumjohann & Glaßmeier, 1984). Global Pi-2 oscillations, alternatively, are the result of plasmaspheric cavity resonance (PCR), a system eigenmode of the plasmasphere (e.g., Yeoman & Orr, 1989; Lin et al., 1991; Takahashi et al., 1995). Since PCR is restricted to plasmaspheric field lines, any adjustment of the PCR leads to the emergence of wave energy in the plasma sheet, effectively escaping from the plasmasphere. Lee and Lysak (1999) defined this phenomenon as plasmaspheric virtual resonance (PVR) (Takahashi et al., 2003; Teramoto et al., 2008). In the PVR model, it is argued that the decrease in the Pi-2 amplitudes occurs outside the plasmasphere (Takahashi et al., 2003). Typically, related oscillation periods are longer than those of the PCR/PVR-Pi-2s (Baumjohann & Glaßmeier, 1984)

and their largest amplitudes lie in the auroral zone, specifically at high latitudes(Samson, 1982).

The timing issue of Pi-2 pulsation from the polar cap to the magnetic equator was conducted by Uozumi et al. (2000). Uozumi et al. (2000) addressed the timing relation to Pi-2 power obtained from the oscillation of the H component. They investigated the relationships between the relative timing of the maximum amplitude of Pi-2 magnetic energy and the latitudinal propagation of Pi-2 perturbations. In their finding, the timing of the maximum power implied the group velocity or group delay, which was used for the examination of the wave energy transfer of Pi-2 pulsations. However, they did not look into the characteristics of longitudinal Pi-2 wave propagation. Uozumi et al. (2004) used the Uozumi et al. (2000) approach to address the characteristics of longitudinal and latitudinal Pi-2 propagation in the auroral zone. The morphology of Pi-2 propagation in high-latitude areas was determined. Nevertheless, this morphology was limited to high-latitude areas and thus, it was insufficient to fully explain Pi-2 propagation on a global scale. Uozumi et al. (2009) clarified the low-latitude and high-latitude timing relations by MLT dependence of the delay time of the auroral Pi-2 for each horizontal component utilizing the low-latitude Pi-2 timing as a reference. The propagation and generation mechanism of these plasma waves is still ongoing. The current study briefly addresses the timing issue by considering both postmidnight and pre-midnight Pi-2 ULF waves globally.

Ground Pi-2 pulsations are composed of several different modal components (Fukunishi, 1975). It is, however, principally challenging to decompose the mixed waveform using the conventional Fourier transform method because of the overlapping frequency ranges. The locality and complexity of natural signals require robust tools to explore their hidden patterns and detect their presence in raw settings. The rapid fluctuation in the phase and frequency of waves poses another challenge. Hence, it is important to introduce techniques that make it possible to separate such mixed signals into individual modal components as ground-observed Pi-2 pulsations. The multifrequency analysis criterion accurately characterizes the time-frequency component of natural signals while preserving their original formation. Therefore, it is a desirable tool for events associated with space activities and wave analysis in general. Wavelet is a powerful analytical tool in the fields of space science, acoustic industry, mathematics, and many other economic sectors. The power of Wavelet to resolve time-frequency resolution measurements and detect intelligence in signals from noise-masked signals with minimum computation power motivated its selection (yang Zeng & guang Wang, 2013).

Wavelet transform applications in space sciences have succeeded significantly in studies of space events. It has been widely used in the denoising of geomagnetic field data (Kumar & Foufoula-Georgiou, 1997; Jach et al., 2006; Xu et al., 2008), the geomagnetic storm initial phase determination (Hafez et al., 2010), the automatic detection of sudden storm geomagnetic onsets (Hafez et al., 2012), in the automatic recognition of Pc5 and Pc3 pulsations using machine learning (Omondi et al., 2023b; Balasis et al., 2019) and the extraction of periodic components caused by the rotation of the Earth. This paper focuses on the automatic detection of Pi-2 pulsations from the ground magnetic field variations associated with the explosive plasma phenomena of auroral substorms. In practice, without pre-determining any modes or frequency range as the norms in the Fourier transform, the wavelet automatically distinguishes anomalies from Pi-2 with no signal distortion (Vetterli, 1986). The wavelet power manifests itself in the ONW data when Pi-2 pulsations are recovered from modulation from sea currents because of the proximity of the ground monitor to the sea. Finally, the causality of Pi-2 ellipticities, time delays, and longitudinal propagation during substorm onset are also investigated. The current paper is organized into five major sections, beginning with the introduction, followed by data and methods, then results, summary and discussion, and finally conclusion.

2 Data and Methods

Our study analyzes the data from the ground-based magnetometer stations in the Circum-pan Pacific Magnetometer Network (CPMN) along 210° magnetic meridians (MM) chain. The data measurements were done by magnetometers as described on the MAGDAS website (`https://data.i-spes.kyushu-u.ac.jp`). In the study, data from 15 monitors were used for Pi-2 pulsation detections (refer to Figure 1 and Table 1). The data sets presented were in unprocessed settings dominated by noise, with ZYK and KOT recording the worst. White noise was dominant in many stations. These noises can be effectively eliminated by the proper application of conventional methods such as low-pass filtering at a given cut-off frequency which requires careful evaluation to perform. These methods have drawbacks and perhaps lead to signal loss in the process of data wrangling. The power of wavelet manifests in signal detection in the presence of noise-infested data. It performs excellently well in anomaly detection and signal discrimination with nearly the same frequency band as the case of the Pi-2 and Pc-4 classes. The two phenomena are related in time-frequency property with different physical oscillation, occurrence duration, and signal energy. Pc-4 for instance is continuous, long occurrence duration, and is linked to different space phenomena occurring outside the inner magnetosphere. While Pi-2 portrays completely different signal aspects suited for inner/outer magnetospheric studies. Using wavelet analytics does not necessarily require much data remediation aside from basic data munging such as formatting or parsing to ensure data is human-machine readable. Table 1 lists CPMN stations and their respective coordinates in both geographic and geomagnetic systems. Where abbreviations; Glat and Glon are the geographic latitude and longitude while GMlat and GMlon are the geomagnetic latitude and longitude respectively. Finally, L is the L-shell value for each respective station.

Table 1. List of CPMN Ground Stations along 210° magnetic meridian

Station	GLat (°)	GLon (°)	GMLat (°)	GMLon (°)	L
KTN	75.94	137.71	69.92	201.03	8.62
TIK	71.59	128.78	65.65	196.90	5.98
CHD	70.62	147.89	64.66	212.14	5.55
ZYK	65.75	150.78	59.60	216.76	3.97
MGD	59.97	150.86	53.49	218.75	2.87
PTK	52.94	158.25	46.17	226.02	2.12
ONW	38.43	141.47	31.15	212.63	1.39
KAG	31.58	130.72	24.37	202.36	1.22
GUA	13.58	144.87	5.61	215.55	1.03
BIK	-1.08	136.05	-9.73	207.39	1.05
EWA	21.32	-158.00	21.63	269.45	1.18
KOT	66.88	-162.60	64.52	249.85	5.49
WEP	-12.68	141.88	-21.93	214.44	1.18
BSV	-25.54	139.21	-36.10	213.08	1.56
CAN	-35.30	149	-45.72	226.29	2.08

In the current study, 1 s data cadence was used for 30 minutes consisted in all stations. This time window was logical for Pi-2 analysis which only happens for a period between 10-15 minutes. Furthermore, the data used for Pi-2 oscillations analysis in the work corresponding to the substorm onsets period occurred at 22.97 MLT, 17th, February 1995 and observed in the geographic location 70.2°, 147.89° (`https://supermag.jhuapl.edu/substorms/`). The substorm onset events of the February 17th were obtained from the Forsyth et al. (2015) substorm onset list. According to the SOPHIE technique, the onset occurred at 13:39 UTC. The topographical map in Figure 1 gives information about

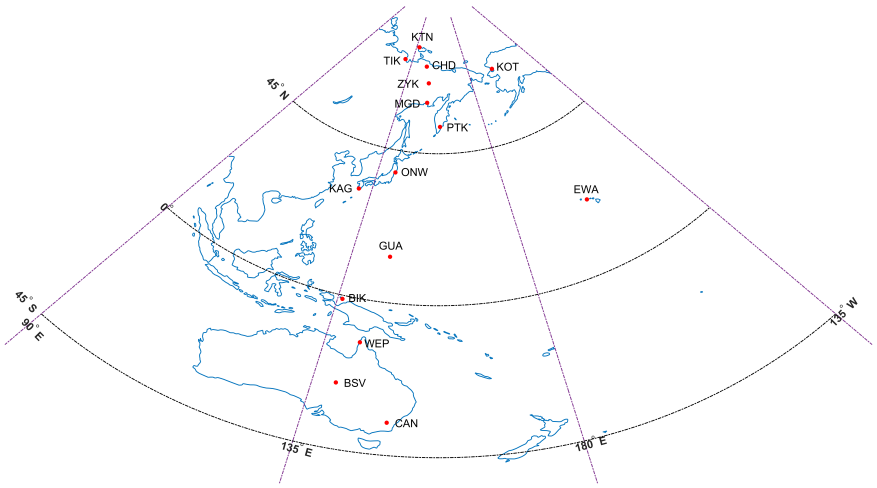

Figure 1. The topographical map of the 210° magnetic meridian MAGDAS magnetometer stations. The latitude and Longitude in the map are expressed in the geodesic coordinate system.

the location of each CPMN station. This CPMN network gives the global view of these Pi-2 ULF wave distributions, the latitudinal wave propagation, and the evolution from Pi-2. The stations' exact locations on the map are marked with red stars.

2.1 Wavelet Analysis

Ground geomagnetic field measurements often consist of many physical component embeddings such as dipole field and perturbations from space. The study of each embed in isolation on the same scale as the original signal requires multiscale approximation or multiresolution analysis. This refers to signal decomposition into individual components in different scales and upon reconstruction can produce the exact single signal as the original signal. Wavelet analysis techniques utilize this method in the detection cases using discrete wavelet transform. Mathematically, ground magnetic perturbations in the realm of wavelet analytics can be conceptualized as follows. Consider a function $f(t)$ as the original signal. If $f(t)$ is a series of approximations of subspaces such that $f(t) \in V_j$ where j is the integer of increasing values, then $f(2t) \in V_{j+1}$. Projecting the function $f(t)$ at each level j onto the subspace V_j, the projection then is defined by the approximation coefficient $C_j[l]$. The inner product of $f(t)$ with the translated and dilated-scaled version of the scaling function $\phi(t)$ is given by Eq.1 (S. G. Mallat, 1989):

$$C_j[l] = \langle f, \phi_{j,l} \rangle = \langle f, 2^{-j}\phi(2^{-j} \cdot -l) \rangle \tag{1}$$

where the scaling function, $\phi(t)$, satisfies the condition described in Eq.2.

$$\frac{1}{2}\phi(\frac{1}{2}t) = \sum_k h(k)\phi(t-k) \tag{2}$$

The expression in Eq.2 permits the direct computation of C_{j+1} from C_j. From C_0 all the coefficients $(C_j[l])_{j>0,l}$ can be calculated without directly invoking any other inner product:

$$C_{j+1}[l] = \sum_k h(k-2l)C_j[k] \tag{3}$$

The number of inner products at each level j is divided by 2. Gradually the signal is smoothed leading to loss of information. The details (low-pass signal) are recovered from the subspace W_{j+1}, which is the orthogonal component of V_{j+1} in V_j. This subspace is generated using wavelet function $\psi(t)$ by dilation and translation (Daubechies, 1988, 1992;

S. Mallat, 2009).

$$\frac{1}{2}\psi(\frac{1}{2}t) = \sum_k g[k]\phi(t-k) \tag{4}$$

The wavelet coefficients are calculated by Eq.5-6

$$\begin{aligned} W_{j+1}[l] = \langle f, \psi_{j+1,l}\rangle &= \langle f, 2^{-(j+1)}\psi(2^{-(j+1)})\cdot -l\rangle \\ &= \sum_k g(k-2l)C_j[k] \end{aligned} \tag{5}$$

$$\begin{aligned} C_{j+1} &= \left[\tilde{h} \star C_j\right] \downarrow_2 \\ W_{j+1} &= \left[\tilde{g} \star C_j\right] \downarrow_2 \end{aligned} \tag{6}$$

To recover the original data, we utilize the properties of orthogonal wavelets. Considering biorthogonal wavelet bases filters $\tilde{g}$ and $\tilde{h}$ (Cohen et al., 1992) are defined to be dual to g and h such that (g, h, $\tilde{g}$, $\tilde{h}$) gives a perfect reconstruction filter bank. Then, the reconstruction of the signal is performed by expression

$$\begin{aligned} C_j[l] = 2\sum_k \left(\tilde{h}[k+2l]C_{j+1}[k] + \tilde{g}[k+2l]W_{j+1}[k]\right) \\ = 2(\tilde{h} \star \tilde{C}_{j+1} + \tilde{g} \star \tilde{W}_{j+1})[l] \end{aligned} \tag{7}$$

where $\tilde{C}_{j+1}$ is zero interpolation of C_{j+1} given by the assertions

$$\begin{aligned} \tilde{C}_{j+1}[l] &= \left[C_{j+1}\right] \uparrow_2 [l] \\ &= \begin{cases} C_{j+1}[m] & \text{if l=2m} \\ 0 & \text{Otherwise} \end{cases} \end{aligned}$$

and the filters $\tilde{g}$ and $\tilde{h}$ must verify the biorthogonal conditions of de-aliasing and exact reconstruction (Vetterli, 1986). Equation 1 to 7 describes the formulations of wavelet multiresolution analysis. Where Morlet continuous wavelet transform and coherence were formulated using the same concept demonstrated in my previous publication(Omondi et al., 2023a).

In the study, we utilized a 1-dimensional multiresolution wavelet decomposition method to decompose data into wavelet decomposition vector v and bookkeeping vector b using level 5 Daubechies wavelet of order 8 (Daubechies, 1992; S. G. Mallat, 1989). To obtain signals, the 1-D wavelet reconstruction method was performed with the v,b, and db8 as the input to the wavelet reconstruction function. In principle, only two signals were possible to reconstruct, that is, the high-frequency component also known as approximations, and the low-frequency counterpart called details. Details were explicitly obtained by specifying the command 'd' as the first input of the wavelet reconstruction function. This is the intelligible waveforms in the spectrum of Pi-2 waves. This step was repeated to reproduce background information as an approximation replacing 'a' in place of 'd' (Daubechies, 1992; Omondi et al., 2023b). Figure 2 & 3 gives vivid visual steps and results of the wavelet analysis technique explored.

Figure 2 summarises Pi-2 pulsation detection processes schematically using pure raw data as the input. For validation of the accuracy of the detection signal, we used the Morlet wavelet to observe the frequency-time property of the Pi-2 pulsations as shown in Figure 2 & 4, for example, (Omondi et al., 2023a, 2023b). The picture of Daubechies wavelet transform as an automatic detection tool was explicitly demonstrated in Figure

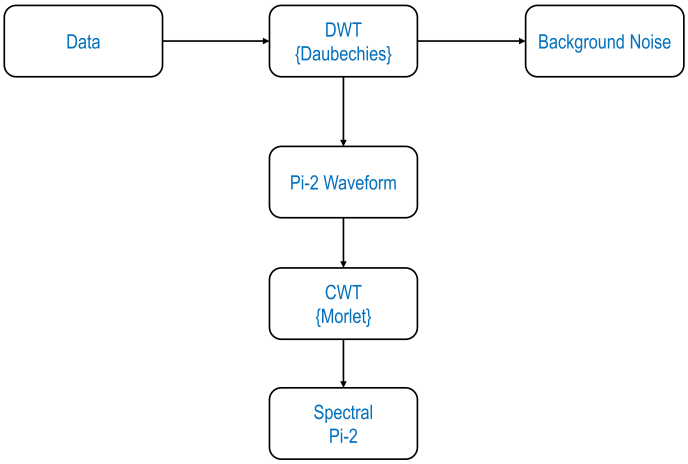

Figure 2. Schematic flowchart diagram illustrating successive stages of Pi-2 pulsation detection using wavelet detection criterion from magnetic field data.

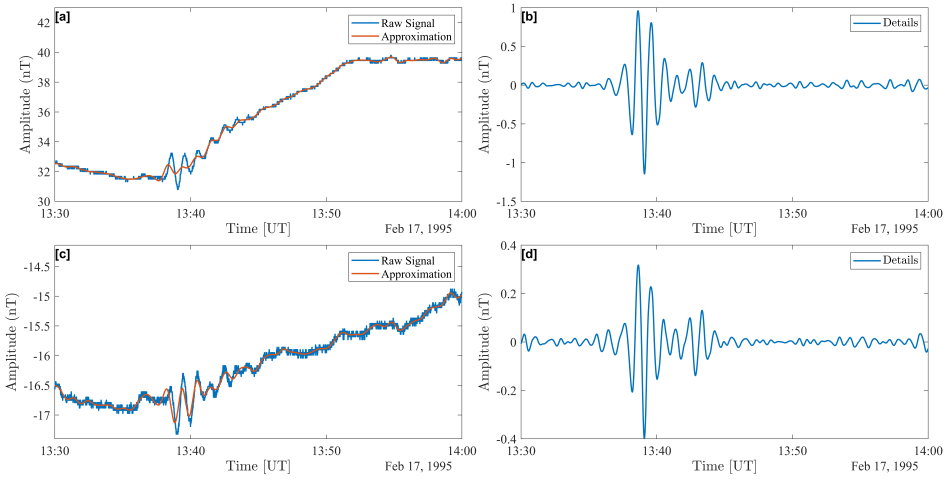

Figure 3. Time series plots of the horizontal component of the magnetic field, the raw data in blue and approximation in orange. Panels (a) & (b) are examinations from CAN and (c) & (d) are from the EWA station. The details and approximation are Pi-2 pulsations and background noise respectively.

3, taking CAN and EWA station H-components as illustrative cases. Where the observations in (a) & (b) are from CAN and (c) & (d) from EWA respectively. Figure 3 (a) & (c) shows the raw magnetic field data in blue and the approximation in orange after wavelet decomposition and reconstruction. The detected Pi-2 waves are shown in Figure 3 (b) & (d). Where UT is the abbreviation for universal time. We can see approximations in panels 3(a) & (c) are highly smoothed and deviate from the raw data having similar trends. It is important to note that this approximation contains many sig-

nal components except one extracted at level 5. These signals are not in the scope of this study and any oscillatory studies such as Pi-1 or Pc3-4 may be present in it and are treated as background noise. The vivid dominant white noise seen in panels 3(a) & (c) can be obtained explicitly by the wavelet analytic denoising method as demonstrated in my previous publication (Omondi et al., 2023b).

3 Results

The classification scheme for observed ground Pi-2 pulsations using latitudinal extents: low, mid, and high latitudes are unclear, and the L-range based division alone is also insufficient (Sutcliffe & Yumoto, 1989). Hence, accounting for Pi-2 pulsations covering more than one L range is highly desirable. The preferred categorization scheme for Pi-2 waves on their physical properties is one proposed by Samson (1982), defining high latitudes as any region influenced by magnetic fields from the ionospheric substorm electrojet. The regions situated latitudinally below are termed mid-latitude regions. This definition gives freedom for the latitudinal motion of the electrojet with geomagnetic conditions. This paper adopted this convention, referring to high latitude ground Pi-2 pulsations as auroral zone Pi-2, and the equatorward as sub-auroral zone Pi-2 (Yeoman & Orr, 1989). With this definition, the plasma sheet field lines are accurately mapped as conjugate to the auroral zone, and the plasma trough and possibly portions of the plasmasphere as a mirror of the sub-auroral zone. The low latitude zones are retained as regions with $L < 2$. The scalograms in Figure 4,5,6,9 and 10 are the automatically detected Pi-2 pulsations by Morlet mother wavelet continuous transformation of the Daubechies discrete wavelet transform (waveforms) from the magnetic field lines of the CPMN stations.

3.1 Sub-Auroral Pi-2 Pulsations

Figures 4-6 illustrate global Pi-2 oscillations in low-latitude observed in the nightside sector. Each panel shows results obtained from the H and D magnetic field components in the corresponding stations in local time (LT). Overall, Pi-2 pulsations recorded in the magnetic field H component in all mid-low latitude stations (Fig. 8) arrived simultaneously with a clear coherent profile suggesting the same wave originating from the same source. Compared to those monitored in the D component, they arrived at different times. Demonstrating interesting findings about the Pi-2 waves and their propagation mechanisms in the magnetosphere during geomagnetic activity along 210° MM. The wavelet scalograms in Figures 4-6 show Pi-2 pulsation of frequency range 6.7-22 mHz consistent in all stations.

Figure 4 presents observations in BIK, GUA, and EWA stations with L-shell values of 1.03 and 1.13 respectively. BIK and GUA are conjugate stations located in opposite hemispheres sharing similar L-values and nearly the same local time. Panels 4(a)-(c) and 4(d)-(f) are Pi-2s detections from the H and D components. The examination of the H component showed clear short transient pulses of damped oscillations with higher amplitudes maximum between 0.3 and 1.5 nT while the D component recorded 0.1 and 0.3 nT spread across three stations. Furthermore, the ULF wave signature in the D panels showed distinct waveform profiles in each station vividly illustrated in scalograms 4(d), (e), and (f). Surprisingly, all the H-components in the three stations oscillated in phase despite their 4-hour difference in local time. The scalograms in H were short-lived compared to the D component in the GUA & BIK observatory. On the contrary, at EWA station which is 1 hour to midnight, smaller waveforms by a factor 5 were detected in both components and were 180° phase shifted in H and D. EWA also recorded similar scalograms as demonstrated in Figure 4(c) & (f). This indicates the localization of Pi-2 pulsation power to a local time. Detailed analysis on Pi-2s polarizations at EWA station is shown in Figure 7.

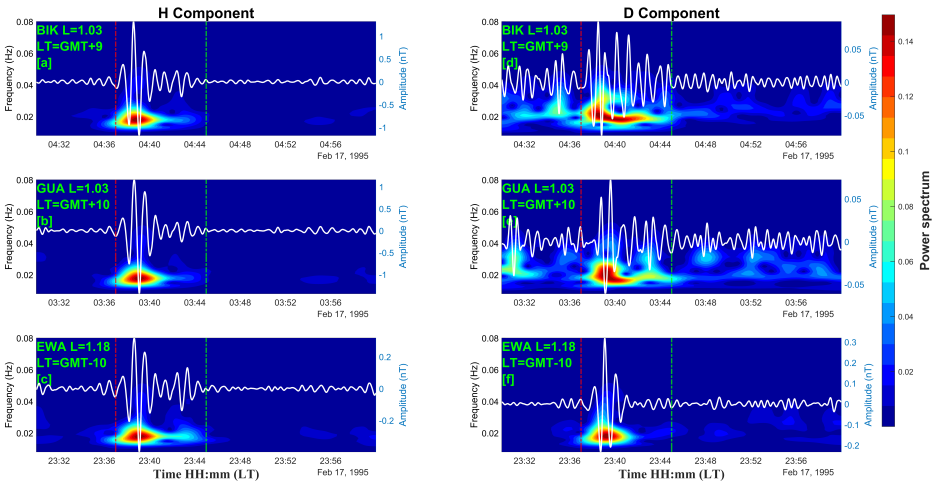

Figure 4. Low latitude Pi-2 pulsation detected BIK, GUA, and EWA. Where (a), (b) & (c) and (d), (e) & (f) are Pi-2 waves recorded in H and D components respectively. The white solid waveform & scalogram are Pi-2 pulsations and the red & green dashed line is Pi-2 duration.

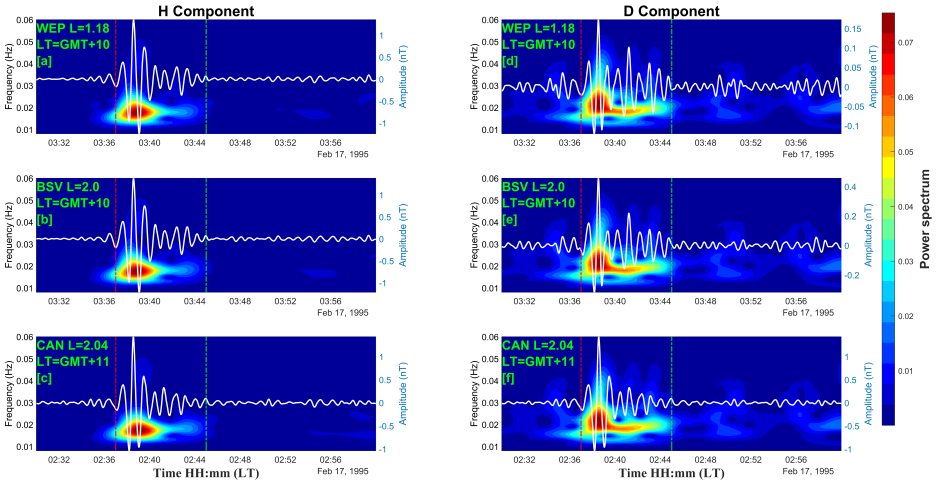

Figure 5. Low Latitude Pi-2 pulsation detected in WEP, BSV, and CAN ground monitors. Where (a), (b) & (c) and (d), (e) & (f) are Pi-2s in H and D components respectively. The white solid waveform & scalogram are Pi-2 pulsations and the red & green dashed line is Pi-2 duration.

Figure 5 demonstrate a special case of Pi-2 waves recorded in WEP, BSV, and CAN stations located in L=1.18, 2.0, and 2.04 respectively. The wave trains in H and D arrived at the same time with coherent wave bays which are in phase at WEP, BSV, and CAN. The Pi-2 wave amplitudes in D magnetic field components are smaller in magnitude in the order of a tenth to those in H at WEP and BSV stations. The Pi-2 profiles in both components are distinct with scalograms in the H component being short while those in D elongated. This invites an interesting question; why would observatories in low to mid-latitude stations located southern hemisphere report unique findings compared to their counterparts? The possibility of Pi-2 source initiation origin and the prop-

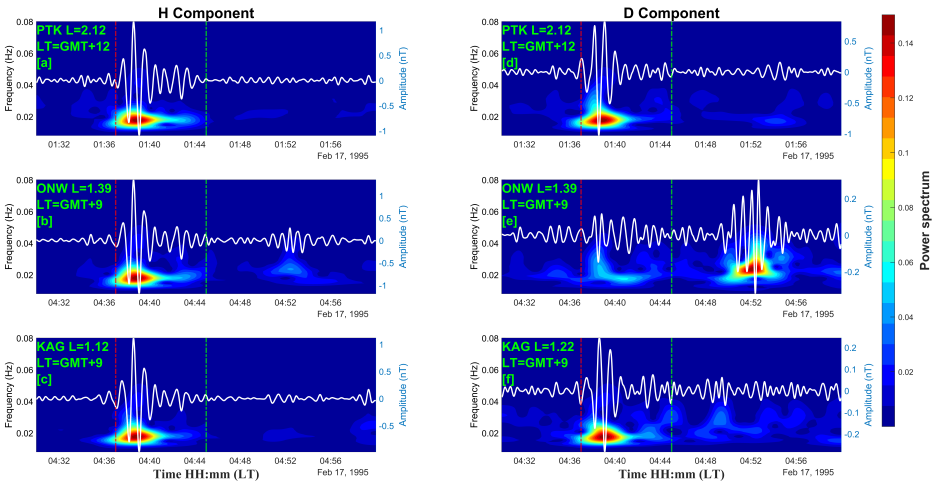

Figure 6. Mid and low-latitude Pi-2 pulsation record from H and D magnetic field components. The KAG, ONW, and PTK stations show comparative observation of Pi-2 oscillations in H and D components in (a)-(f). The red and green dashed lines correspond to the detected Pi-2 Pulsations

agation media perhaps are directly linked to this observation. The northern auroral zone stands to be a location where Pi-2 originated and was more disturbed as Pi-2s are distributed along 210 MM globally.

Figure 6 shows the observations from the PTK, ONW, and KAG observatories in their local time with L-values 2.12, 1.39, and 1.12 respectively. The wave response on the H component arrives simultaneously with the same wave bays in all stations. All wave profiles in the D component are reversed. Dominance of external effects such as local sea currents heavily attenuated the signal arriving at the ONW station in the D component. Hence, results in weak Pi-2 signal reception on the azimuthal component as illustrated in the waveform and scalogram. The Pi-2 pulsation was modulated by the sea currents due to ONW's proximity to the sea (e.g., Romero et al., 2020). It was noted that Pi-2 power dominated more on the H as the D component was severely attenuated and more likely modulated by local effects. Regardless, the recovered signal in D showed a similar pattern in all three stations. It was uniquely observed that Pi-2 waves in both magnetic components were 180° out of phase with H having a higher amplitude than those in D. This implies that the latitudinal profiles of Pi-2 perturbation consist of different mode oscillations.

Pi-2 wave evolution and polarization in H and D magnetic field components during pre-substorm, substorm onset, and post-substorm periods in EWA stations are shown in Figure 7. In the pre-substorm and post-substorm periods, the Pi-2 signal arrived at EWA with a slight phase difference in both components with the H leading as shown in R1 & R2 of Figure 7(a). In the substorm expansion phase, the Pi-2 oscillations evolved with 180° out of phase as in R3 with a peak amplitude at 23:39 LT. This is demonstrated by the horizontal arrows panel 7(b) corresponding to a phase shift of π projected in a unit circle. This polarisation lasted for about 10 minutes. There were similar observations in the PTK, ONW, and KAG in reverse (Fig. 6). Time-frequency consistency and phase difference of Pi-2 pulsations illustrated in Figure 7(b) were consistent with observations demonstrated in Figure 7(a). The small arrows in phase-frequency coherence analysis in Figure 7(b) represent the phase angle between the two signals. The H and D demon-

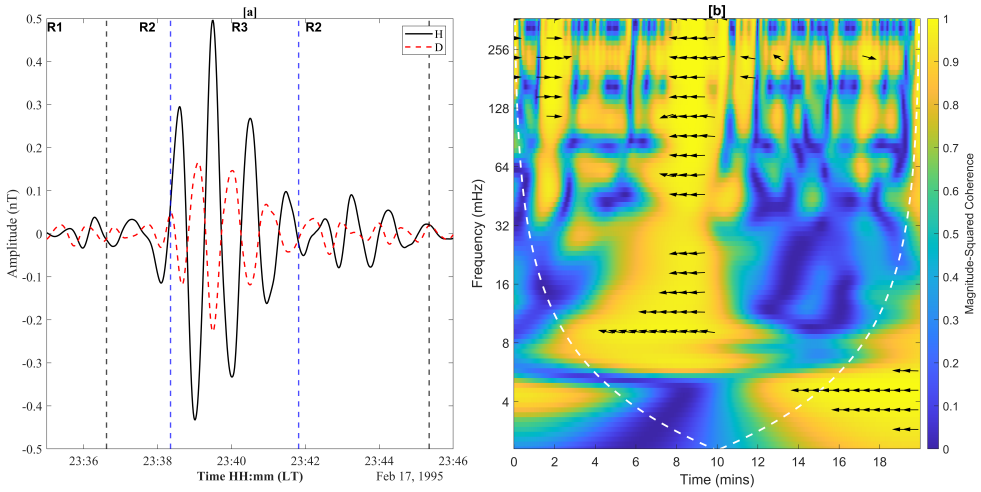

consistent

Figure 7. Pi-2 Pulsation observed in H and D components from EWA ground monitor. (a) illustrates the Pi-2 phase shift and evolution between two magnetic components. (b) shows the wavelet frequency and phase coherence of signals in (a). Where Pi-2 ripples from H and D are in a black solid line and a red dashed line respectively. The blue and black vertical dashed lines show the partition between the region of Pi-2 wave evolution marked by R1, R2, and R3. Finally, the black arrows in panel (b) show phase shift. In principle, vertical arrows show phase lag on a unit circle corresponding to a $\frac{\pi}{2}$. Therefore, the corresponding phase lag of π in panel (b) is consistent with that in panel (a).

strated a high-frequency coherence in the substorm expansion period lasting for 10 minutes beginning from the second minute from the left of panel 7(b).

Figure 8 illustrates the physical properties of Pi-2 wave trains detected in middle and low-latitude stations along 210° MM. In Figure 8 (a) all Pi-2 oscillations beating these regions showed similar wave profiles. These oscillations arrived at 13:37 UT peaking at 13:39:11 UT and gradually decayed. The observations in Figure 8 (b) show that the ultra-low frequency waves of the Pi-2 type delayed arriving at different times in some stations. These D-component waves showed different properties with some peaking simultaneously earlier while some later taking 13:37 UT as the arrival time with CAN and PTK as reference. This unique feature hints at the magnetospheric structure and wave propagation time. To visualize the underlying unique properties of the Pi-2 undulation in Figure 8. The latitude dependence of the Pi-2 pulsations picture and patterns are projected in Figure 8(b).

3.2 Auroral Pi-2 Pulsations

Figures 9 and 10 illustrate nightside Pi-2 undulations observed in the auroral zone. Figure 9 presents the observations in the ZYK, MGD, and KOT stations located at L = 3.97, L = 2.87, and L = 5.41, respectively. There was a phase shift in observations between ZYK and MGD ground monitors as well as in their components despite sharing the same local time. From Table 1 we note ZYK is east of MGD. The negative D oscillations indicate the center of the substorm current wedge is located west of these two monitors(Clauer & McPherron, 1974). The positive H at MGD implies that the downward field-aligned current section of the wedge is situated east of the station. Focusing

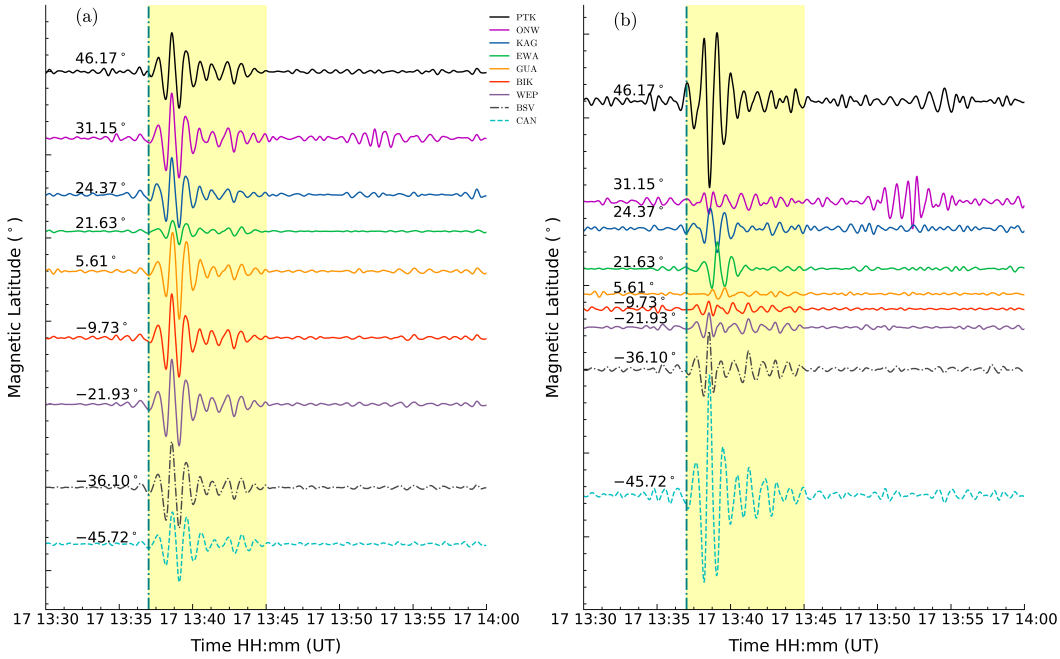

Figure 8. Sub-auroral Pi-2 pulsation waveforms. (a) and (b) shows the H and D perturbations respectively. The H component responded with similar Pi-2 waveforms and amplitude spanning from -45.72° to 46.17° magnetic latitude except for EWA and all peaking at 13:39:11 UT. Similarly, the D component recorded the same waveform in the northern hemisphere stations(46.17°, 31.15°,24.37° & 5.61°) except 21.63° while waves in the southern hemisphere phase reversed in D peaking at 13:38:42 UT. Teal dashed-dotted lines correspond to the detected Pi-2 Pulsations onset while the faint yellow shade is the Pi-2s duration.

on ZYK, Pi-2 ripples arrive delayed by 2 minutes in both magnetic components with a phase reversal of 180°. The ZYK and KOT stations recorded high Pi-2 pulsations amplitudes in both magnetic components with ZYK having 2 nT and KOT 6 nT in the horizontal magnetic component and 1 nT and 2 nT in the D components respectively. MGD responded similarly to those in midlatitude zones with enhanced Pi-2 wave amplitude of 1.5 nT and 1 nT in H and D respectively. In the auroral zone, Pi-2s were observed in KTN, TIK, and CHD observatories located at L=8.62, 5.98, and 5.55 respectively. Figure 10 illustrates the examinations in H and D magnetic components. whereby, Pi-2 oscillations presented various wave profiles localized in each observatory and were completely different from those observed in the sub-auroral regions. Furthermore, the wave morphology scalograms were unique in the three stations both in H and D magnetic field components. Therefore, probably suggests that the wave source and propagation medium are unique and localized for each region. The three wave signals arrived at different times for both components as shown in Figure 10. The wave amplitude in the KTN H panel is twice that in the D panel. TIK recorded a maximum of 5 nT and -4 nT in amplitudes while CHD 5 nT and -10 nT respectively. Overall, all signals presented different spectra, scalograms and with -10 nT and 15 nT peak amplitudes. Figure 11 describes the Pi-2 wave profile in mid-high magnetic latitude. It was observed that the wave profile evolves as it propagates from the auroral to the sub-auroral zone. This wave evolution is visible in all frequencies and amplitude in both magnetic field components signifying the nature of their propagation path in the magnetosphere and ionosphere. Amplitude changes are well shown in Figure 12. The latitudinal and amplitude relationship of Pi-2 magnetohydrodynamic waves globally are illustrated in Figure 12. These observations,

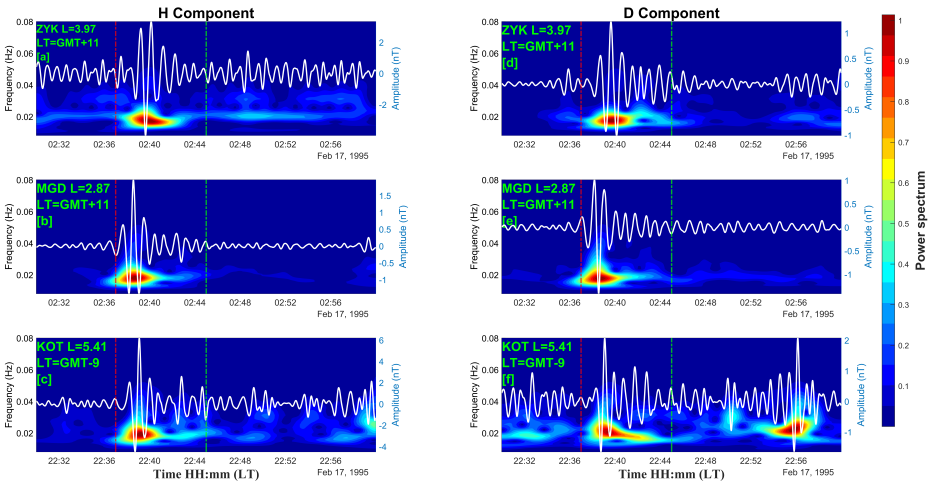

Figure 9. Mid-high latitude Nightside Pi-2 pulsation detected in ZYK, MGD, and KOT stations in H and D components. The red and green dashed lines show the span of detected Pi-2 pulsations.

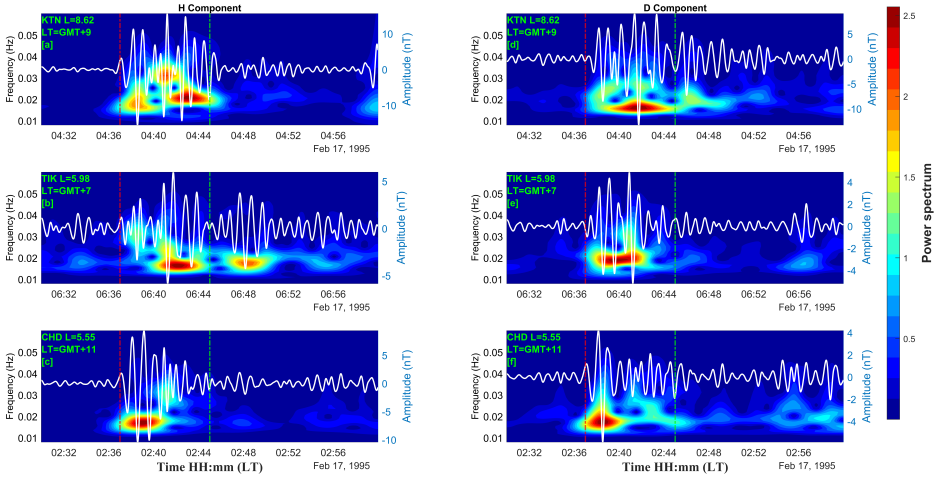

Figure 10. High latitude Pi-2 pulsation detected in KTN, TIK, and CHD stations in H and D components. The red and green dashed lines correspond to the detected Pi-2 Pulsations.

present global wave activities in the H and D components of the magnetic fields. Generally, there was a gradual decrease in Pi-2 pulsation activities equatorward from the zones of auroral brightness intensification along 210° MM. The sharp break in the trend accompanied by an increase in amplitude at CHD compared to TIK indicates a bizarre activity interesting for this study. Overall, The Horizontal component in all latitudes responded with high amplitudes compared to the D components.

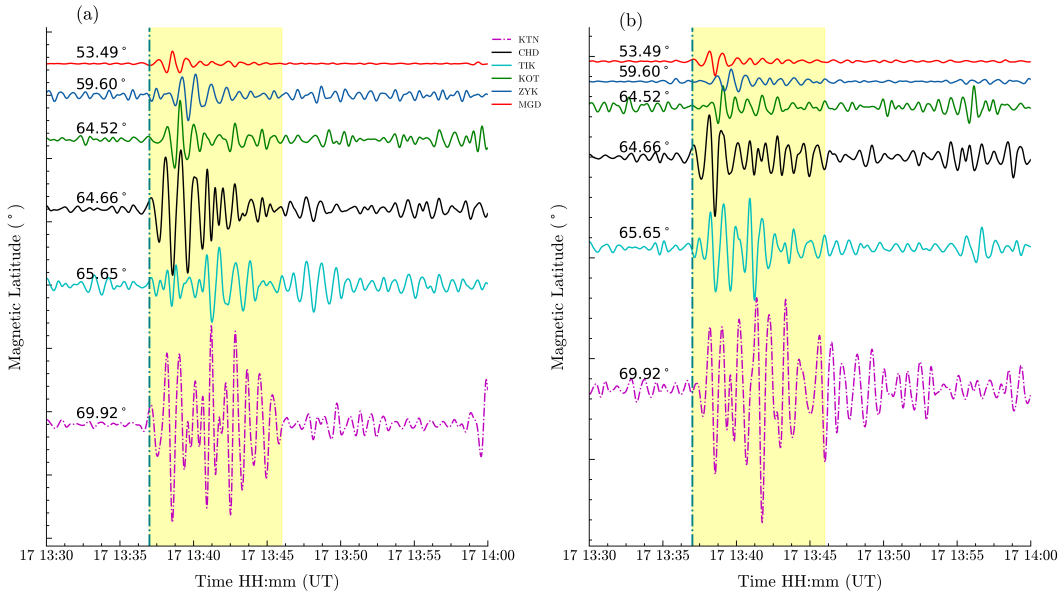

Figure 11. High and mid latitude Pi-2 pulsation waveforms. (a) and (b) shows the H and D perturbations respectively. Collectively, all Pi-2 ULF waves monitored in high latitudes exhibited different wave profiles. Teal dashed-dotted lines correspond to the detected Pi-2 Pulsations onset while the faint yellow shade is the Pi-2s duration.

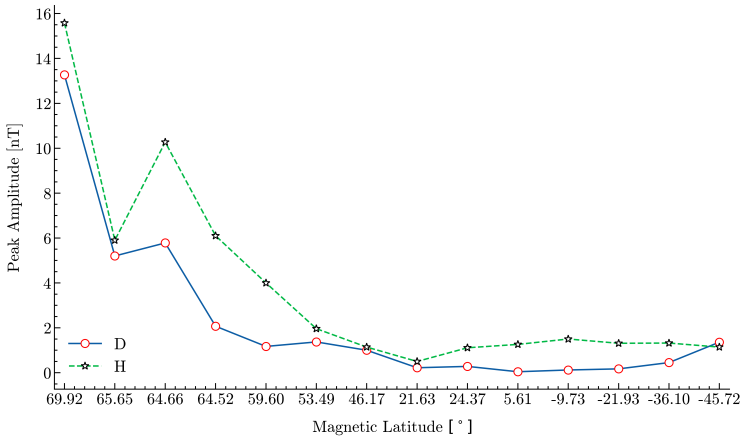

Figure 12. Latitudinal profile of Pi-2 amplitude along 210° MM. Pi-2 absolute amplitude decreases with the decline in absolute magnetic latitude.

4 Summary and Discussion

The characteristics of Pi-2 pulsations observed in the auroral to sub-auroral zone using ground magnetometer data obtained from the CPMN along 210° MM were carefully analyzed. The low-latitude Pi-2 pulsations arrived at 13:37:00 UT, 2 minutes earlier in most observatories in both hemispheres compared to the predicted time of substorm onset, 13:39:00 UT. Consequently, similar observations in H-components of KTN and CHD observatories were detected. These high correlation global Pi-2 events monitored on the nightside in a wide latitudinal and narrow magnetic meridian constituted highly consistent waveforms. Similarly, the same observations were also reported by Keiling et al. (2014a); Uozumi et al. (2009, 2011, 2016a) on their work. Uozumi et al. (2009) stud-

ies on high latitude in the pre-midnight sector resolve to a similar systematic delay in horizontal components and strong Pi-2 pulsations MLT dependence. These wave properties in the auroral zone are strong indicators of forced Alfven waves excited by fast magnetosonic waves (Uozumi et al., 2009). However, the Observatories such as TIK and ZYK exhibited a common time delay of about 2 minutes in their H components compared to those in the low-latitude stations (refer Figure 8 and 11). The delay in Pi-2 arrival in the auroral zone is due to differences in mode conversion and distinct propagation paths. Fast mode waves propagating in the azimuthal direction in the magnetosphere can excite field-aligned mode waves(Alfven waves) on the field lines away from the source region as in the case of the KOT station.

The underlying relationship between KTN, CHD, and ZYK to low latitude ground monitors in terms of observed Pi-2 wave properties is complex. In other studies, however, global Pi-2 pulsations have a single period, while spanning the equatorial to auroral zone with their largest amplitude at high latitudes. This implies that their source lies beyond the plasmasphere (outer magnetosphere). Therefore, to distinguish these waves from the global Pi-2 associated with the global PCR/PVR-Pi-2 pulsations types, they are named super global Pi-2s. The source generation mechanism differentiates super global Pi-2s from Pi-2s types with different periods occurring simultaneously from low to high latitudes. Li et al. (1998) reported Pi-2 events that displayed two periods at different latitudes and argued that the transient response mechanism operated in the high latitudes while PCR in the low and mid-latitudes (Keiling et al., 2014b). However, for super global Pi-2, it was suggested that only one generation mechanism operated, even if with numerous different propagation conduits from their source to the ground(e.g., Uozumi et al., 2009). On the other hand, sub-auroral global Pi-2 pulsations have also been explained initially by cavity resonance(Takahashi et al., 1999). It was pointed out that in principle, these Pi-2 waves are triggered by forced driving of the system. Other observational evidence on the forcing mechanism argued that the observed sub-auroral Pi-2 oscillations were driven by velocity modulations in fast plasma flows (BBF) in the central plasma sheet, which would subsequently couple to MHD waves in the plasmasphere (inner magnetosphere). Keiling et al. (2008) proposed high-latitude forcing showing evidence that some ground Pi-2 waves are directly controlled by the reconnection site also known as reconnection-driven Pi-2 pulsations. While the source for the BBF-driven Pi-2s is connected to tail reconnection. Thus, the propagation model must be different compared to that of the reconnection-driven Pi-2 model. The latter suggested that besides the flow modulations in the plasma sheet, Alfvénic variation on high-latitude flux tubes carried the Pi-2 signal faster to high latitudes on the ground, where Pi-2s were first spotted. Therefore, associating monochromatic Pi-2 pulsations observed in the sub-auroral as super global Pi-2 is logical.

The phase reversal (180 ° out of phase) between ZYK and CHD with corresponding L-values of 3.97 and 5.55 indicates the plasmapause location. For certainty, this observation syncs with Tokunaga et al. (2007) results showing they are probably situated along the plasmapause boundary during the Pi-2 pulsation event. Polarization reversal of substorm-related Pi-2 undulations near plasmapause has been generally accepted by many researchers (e.g., Fukunishi, 1975). Takahashi et al. (2003) described the events occurring near the plasmapause at CRRES (Combined Release and Radiation Effects Satellite) using the phase of compressional component (Bz) to be assembled both at 0 ° and 180 °. Their observations pointed out a consistent trend with the cavity mode according to a numerical simulation using a realistic plasmapause plasma density structure and a dipole magnetic field, which shows that the node of Bz is situated near the plasmapause. CHD and TIK lie nearly along the same latitude with a difference of 15° and 19° in magnetic and geographic longitudes respectively. Therefore, it was expected to record phase-coherent signals. On the contrary, anti-phase signals were monitored in instead. Hence, the phase shift between CHD and TIk arguably comes from the longitudinal tunneling of fast mode waves in the high latitude (Uozumi et al., 2004). Tokunaga

et al. (2007) studied the azimuthal wave number of the Pi-2s from these stations and found it to be about 3 which syncs with those obtained from high latitude regions as reported in previous works(e.g., Lester et al., 1983). In addition, the waveforms in CHD H and D components are noted to be slightly different with enhanced amplitudes. Thus, we suggest that the D and H fluctuations at the CHD station are initiated by a common source but with different generation mechanisms. Pi-2 waves in the CHD H component recording higher amplitudes are caused by FAC oscillations, i.e., field line resonance (Kim et al., 2005) while in the D perturbations are contributed by a combination of fast waves and FAC oscillations. This probably explains the shoot in Pi-2 amplitude compared to the TIK breaking the trend (refer to Figure 12) (Tokunaga et al., 2007).

Pi-2 pulsations detected in the sub-auroral zone lasted for about 10 minutes with similar H-bays arriving simultaneously with different wave profiles in D. The presence of group delays in the D components was also reported by other authors in their studies (e.g., Webster et al., 1989; Li et al., 1998; Hsu & McPherron, 2007). These Pi-2 beatings are manifestations of fast Alfven waves in the geomagnetic northward and FAC oscillations in the geomagnetic eastward (D) components. Subsequent increasing trends in amplitude from the equatorial to the auroral zone evidence wave power couplings or transfer into the L-shells away from the energy source (Saito, 1969; Rostoker & Samson, 1981). Fast mode waves driving Pi-2 magnetohydrodynamics waves in the lower latitudes require a longer time window to propagate through the plasmasphere. Hence causing smaller amplitudes in zones within $L \leq 2$. On the other hand, consistent and nearly monochromatic spectral patterns of Pi-2 pulsations in the sub-auroral zone were observed. It was proposed that early Pi-2s arriving on the northern components were triggered by fast-mode cavity resonance (PCR/PVR) as the generation mechanism rather than a periodic forcing by freely propagating fast-mode waves. It is also suggested that (PVR/PCR) cavity resonances are incapable of driving large amplitudes in the auroral zone (Takahashi et al., 2003). Interestingly WEP, BSV, and CAN detected the same Pi-2 pulses in both components. Furthermore, Similar H-bays and D-bays were observed with nearly the same amplitudes in H disturbances and exponentially increasing in D beats from WEP to CAN (refer to Figure 8 and 12). Therefore, global-mode oscillation must be associated with these components in the inner magnetosphere. A similar finding was also reported in their group studies on characteristics of low-latitude Pi-2 pulsations (Yumoto et al., 2001).

WEP and EWA in the low latitude region are located on opposite sides, where WEP is east of EWA with an exact time difference of 10 hours. Despite being along the same magnetic latitude, the Pi-2 pulsations recorded in them differ in both components. In EWA there was a clear wave polarisation while WEP reported none. This illustrates the latitudinal propagation of the Pi-2 wave property. The ellipticity in EWA as characterized in Figure 7 are direct consequence of surface waves generated by injection trajectories with distinct particle energies and flow diversions (Saka et al., 2010). On the other hand, the polarization of Pi-2 pulsations in PTK, ZYK, and MGD in the midlatitude zone was associated with phase modulation due to overhead currents (Uozumi et al., 2016b). There are two possible situations for this kind of polarisation occurring in the mid-latitude region; the transient response Pi-2 and PCR-Pi-2 (Allan et al., 1996). In the PCR model, the meridian of the fast-mode source coincides with the center meridian of the polarization pattern triggering the cavity while in the transient response model, the upward current of the Substorm Current Wedge is close to the center meridian (Uozumi et al., 2016a). Therefore, in PTK and MGD, the center meridian was close to 210° which is also coherent with the Lester et al. (1983) findings. The observation in the auroral zone demonstrates a modulation of Pi-2 pulsations scaling with an increase in L- value maximum at KTN and minimum in KOT. The influence of external effects such as local sea currents heavily attenuated the signal arriving at the ONW station in the D component. Therefore, the wave power in the H-component was stable and resistant to local effects while those in D were susceptible implying received Pi-2s are less energetic. The Pi-2 pulsation modulation by the sea currents due to ONW's proximity to the sea shows the need

to factor external influences in Pi-2 analysis aside from noise. This observation portrays the Pi-2 reception powers and local influences at D components compared to H counterparts making the wavelet technique a useful tool in analysis.

5 Conclusion

In summary, the ground Pi-2 Pulsations detected in the 210° MM network consisted of various irregular modal components indicating the tunneling of shear and fast Alfven waves, field line resonances, and finally plasmaspheric resonances. The influences of local effects such as sea currents are also emphasized affecting the reception of Pi-2 signals in some monitors in the CPMN network. Thus, highlighting the consequence of considering local environmental effects in data analysis. During the onset of the substorm expansion, the near-Earth magnetotail suddenly reconfigured to a dipole state from its original physical state of stretched configuration. The change in the magnetosphere configuration is instigated by the formation of the substorm current wedge (SCW), when the cross-tail current gets short-circuited to the auroral ionosphere via field-aligned currents, due to the disruption of the tail current. Pi-2 pulsations are regarded as the manifestation of the sudden change in the state of the magnetosphere during a substorm, which can be monitored at different radial distances from the Earth's surface. In conclusion, this study provides valuable insights into the features of Pi-2 pulsations in the sub-auroral to the auroral zone. Their latitudinal and longitudinal propagation and initiation mechanisms. Finally, their variations across different magnetic latitudes along narrow meridians. The association of Pi-2 pulsations with substorms is an important proxy for understanding the coupling process between the magnetosphere-ionosphere coupling and the complex electrodynamic processes in the magnetosphere. The successful application of the wavelet analytic detection technique of Pi-2 pulsation in the current study makes it a valuable tool for future research in the magnetospheric community. Mapping global simulations with ground observations to complement limited space observations would provide a comprehensive understanding of mixing systems in the ionospheric and magnetosphere.

Acknowledgments

This work was collaboratively supported by the Scientific Committee on Solar-Terrestrial Physics (SCOSTEP) SVS program and the International Research Center for Space and Planetary Environmental Science (i-SPES or ICSWSE) in Kyushu University under PI Prof.Akimasa Yoshikawa. The data were provided by the principal investigator of the MAGDAS/CPMN project `http://magdas.serc.kyushu-u.ac.jp/`. I extend my humble gratitude to the SCOSTEP team and i-SPES research group for their joint support for my 3 months visit and research in Japan. I acknowledge the generosity and well-being provided by the Japanese research colleagues for my happy stay and Japanese experience. I also appreciate the involuntary support provided by Egypt Japan University of Science and Technology in facilitating my visit to and from Japan through Prof. Ayman Mahrous. The author gives much appreciation to the MAGDAS team for their effort and dedication in maintaining and making MAGDAS/CPMN magnetic data available for public use.

References

Allan, W., Menk, F., Fraser, B., Li, Y., & White, S. (1996). Are low-latitude pi2 pulsations cavity/waveguide modes? *Geophysical research letters*, *23*(7), 765–768.

Balasis, G., Aminalragia-Giamini, S., Papadimitriou, C., Daglis, I. A., Anastasiadis, A., & Haagmans, R. (2019). A machine learning approach for automated ulf wave recognition. *Journal of Space Weather and Space Climate*, *9*, A13.

Baumjohann, W., & Glaßmeier, K.-H. (1984). The transient response mechanism and pi2 pulsations at substorm onset—review and outlook. *Planetary and Space Science*, *32*(11), 1361–1370.

Clauer, C. R., & McPherron, R. L. (1974). Mapping the local time-universal time development of magnetospheric substorms using mid-latitude magnetic observations. *Journal of Geophysical Research*, *79*(19), 2811–2820.

Cohen, A., Daubechies, I., & Feauveau, J.-C. (1992). Biorthogonal bases of compactly supported wavelets. *Communications on pure and applied mathematics*, *45*(5), 485–560.

Daubechies, I. (1988). Orthonormal bases of compactly supported wavelets. *Communications on Pure and Applied Mathematics*, *41*(7), 909-996. doi: https://doi.org/10.1002/cpa.3160410705

Daubechies, I. (1992). *Ten lectures on wavelets*. SIAM.

Forsyth, C., Rae, I., Coxon, J., Freeman, M., Jackman, C., Gjerloev, J., & Fazakerley, A. (2015). A new technique for determining substorm onsets and phases from indices of the electrojet (sophie). *Journal of Geophysical Research: Space Physics*, *120*(12), 10–592.

Fukunishi, H. (1975). Polarization changes of geomagnetic pi 2 pulsations associated with the plasmapause. *Journal of Geophysical Research (1896-1977)*, *80*(1), 98-110. doi: https://doi.org/10.1029/JA080i001p00098

Hafez, A. G., Ghamry, E., Yayama, H., & Yumoto, K. (2012). A wavelet spectral analysis technique for automatic detection of geomagnetic sudden commencements. *IEEE Transactions on Geoscience and Remote Sensing*, *50*(11), 4503-4512. doi: 10.1109/TGRS.2012.2192279

Hafez, A. G., Khan, M. T. A., & Kohda, T. (2010). Clear p-wave arrival of weak events and automatic onset determination using wavelet filter banks. *Digital Signal Processing*, *20*(3), 715-723. doi: https://doi.org/10.1016/j.dsp.2009.10.002

Hsu, T.-S., McPherron, R., Angelopoulos, V., Ge, Y., Zhang, H., Russell, C., ... Kissinger, J. (2012). A statistical analysis of the association between fast plasma flows and pi2 pulsations. *Journal of Geophysical Research: Space Physics*, *117*(A11).

Hsu, T.-S., & McPherron, R. L. (2007). A statistical study of the relation of pi 2 and plasma flows in the tail. *Journal of Geophysical Research: Space Physics*, *112*(A5). doi: https://doi.org/10.1029/2006JA011782

Jach, A., Kokoszka, P., Sojka, J., & Zhu, L. (2006). Wavelet-based index of magnetic storm activity. *Journal of Geophysical Research: Space Physics*, *111*(A9). doi: https://doi.org/10.1029/2006JA011635

Keiling, A., Marghitu, O., Vogt, J., Amm, O., Bunescu, C., Constantinescu, V., ... Sorbalo, E. (2014a). Magnetosphere-ionosphere coupling of global pi2 pulsations. *Journal of Geophysical Research: Space Physics*, *119*(4), 2717-2739. doi: https://doi.org/10.1002/2013JA019085

Keiling, A., Marghitu, O., Vogt, J., Amm, O., Bunescu, C., Constantinescu, V., ... others (2014b). Magnetosphere-ionosphere coupling of global pi2 pulsations. *Journal of Geophysical Research: Space Physics*, *119*(4), 2717–2739.

Keiling, A., Mozer, F., Reme, H., Dandouras, I., Lucek, E., Fujimoto, M., ... Reeves, G. (2008). Periodic traveling compression regions during quiet geomagnetic conditions and their association with ground pi2. In *Annales geophysicae* (Vol. 26, pp. 3341–3354).

Keiling, A., & Takahashi, K. (2011). Review of pi2 models. *Space Science Reviews*, *161*, 63–148.

Kepko, L., Kivelson, M., & Yumoto, K. (2001). Flow bursts, braking, and pi2 pulsations. *Journal of Geophysical Research: Space Physics*, *106*(A2), 1903–1915.

Kim, K.-H., Lee, D.-H., Denton, R.-E., Takahashi, K., Goldstein, J., Moon, Y.-J., ... Keiling, A. (2005). Pi2 pulsations in a small and strongly asymmetric

plasmasphere. *Journal of Geophysical Research: Space Physics*, *110*(A10).

Kumar, P., & Foufoula-Georgiou, E. (1997). Wavelet analysis for geophysical applications. *Reviews of Geophysics*, *35*(4), 385-412. doi: https://doi.org/10.1029/97RG00427

Lee, D.-H., & Lysak, R. L. (1999). Mhd waves in a three-dimensional dipolar magnetic field: A search for pi2 pulsations. *Journal of Geophysical Research: Space Physics*, *104*(A12), 28691–28699.

Lester, M., Hughes, J. W., & Singer, H. J. (1983). Polarization patterns of pi 2 magnetic pulsations and the substorm current wedge. *Journal of Geophysical Research: Space Physics*, *88*(A10), 7958–7966.

Li, Y., Fraser, B. J., Menk, F. W., Webster, D. J., & Yumoto, K. (1998). Properties and sources of low and very low latitude pi2 pulsations. *Journal of Geophysical Research: Space Physics*, *103*(A2), 2343-2358. doi: https://doi.org/10.1029/97JA02921

Lin, C., Lee, L., & Sun, Y. (1991). Observations of pi 2 pulsations at a very low latitude (l= 1.06) station and magnetospheric cavity resonances. *Journal of Geophysical Research: Space Physics*, *96*(A12), 21105–21113.

Mallat, S. (2009). *A wavelet tour of signal processing, chapters 1 and 12.* Academic Press Chicago.

Mallat, S. G. (1989). A theory for multiresolution signal decomposition: the wavelet representation. *IEEE Transactions on pattern analysis and machine intelligence*, *11*(7), 674–693. doi: 10.1109/34.192463

Omondi, S., Yoshikawa, A., Zahra, W. K., Fathy, I., & Mahrous, A. (2023a). Alex magnetometer and telluric station in egypt: First results on pulsation analysis. *Advances in Space Research*, *72*(3), 711-725. (Space and Geophysical Observations and Recent Results related to the African Continent) doi: https://doi.org/10.1016/j.asr.2022.09.014

Omondi, S., Yoshikawa, A., Zahra, W. K., Fathy, I., & Mahrous, A. (2023b). Automatic detection of auroral pc5 geomagnetic pulsation using machine learning approach guided with discrete wavelet transform. *Advances in Space Research*, *72*(3), 866-883. doi: https://doi.org/10.1016/j.asr.2022.06.063

Romero, L., Hypolite, D., & McWilliams, J. C. (2020). Submesoscale current effects on surface waves. *Ocean Modelling*, *153*, 101662.

Rostoker, G., & Samson, J. C. (1981). Polarization characteristics of pi 2 pulsations and implications for their source mechanisms: Location of source regions with respect to the auroral electrojets. *Planetary and Space Science*, *29*(2), 225-247. doi: https://doi.org/10.1016/0032-0633(81)90036-2

Saito, T. (1969). Geomagnetic pulsations. *Space Science Reviews*, *10*(3), 319–412.

Saka, O., Hayashi, K., & Thomsen, M. F. (2010). First 10 min intervals of pi2 onset at geosynchronous altitudes during the expansion of energetic ion regions in the nighttime sector. *Journal of Atmospheric and Solar-Terrestrial Physics*, *72*, 1100-1109.

Sakurai, T., & Saito, T. (1976). Magnetic pulsation pi2 and substorm onset. *Planetary and Space Science*, *24*(6), 573–575.

Samson, J. (1982). Pi 2 pulsations: High latitude results. *Planetary and Space Science*, *30*(12), 1239-1247. doi: https://doi.org/10.1016/0032-0633(82)90097-6

Singer, H. J., Hughes, W. J., Fougere, P. F., & Knecht, D. J. (1983). The localization of pi 2 pulsations: Ground-satellite observations. *Journal of Geophysical Research: Space Physics*, *88*(A9), 7029-7036. doi: https://doi.org/10.1029/JA088iA09p07029

Sutcliffe, P. R., & Yumoto, K. (1989). Dayside pi 2 pulsations at low latitudes. *Geophysical research letters*, *16*(8), 887–890.

Sutcliffe, P. R., & Yumoto, K. (1991). On the cavity mode nature of low-latitude pi 2 pulsations. *Journal of Geophysical Research: Space Physics*, *96*(A2), 1543–1551.

Takahashi, K., Hughes, W., Anderson, R., & Solovyev, S. (1999). Crres satellite observations associated with low-latitude pi2 pulsations. *Journal of Geophysical Research: Space Physics*, *104*(A8), 17431–17440.

Takahashi, K., Lee, D.-H., Nosé, M., Anderson, R. R., & Hughes, W. J. (2003). Crres electric field study of the radial mode structure of pi2 pulsations. *Journal of Geophysical Research: Space Physics*, *108*(A5).

Takahashi, K., Ohtani, S.-i., & Anderson, B. J. (1995). Statistical analysis of pi 2 pulsations observed by the ampte cce spacecraft in the inner magnetosphere. *Journal of Geophysical Research: Space Physics*, *100*(A11), 21929–21941.

Teramoto, M., Nosé, M., & Sutcliffe, P. (2008). Statistical analysis of pi2 pulsations inside and outside the plasmasphere observed by the polar orbiting de-1 satellite. *Journal of Geophysical Research: Space Physics*, *113*(A7).

Tokunaga, T., Kohta, H., Yoshikawa, A., Uozumi, T., & Yumoto, K. (2007). Global features of pi 2 pulsations obtained by independent component analysis. *Geophysical Research Letters*, *34*(14). doi: https://doi.org/10.1029/2007GL030174

Uozumi, T., Abe, S., Kitamura, K., Tokunaga, T., Yoshikawa, A., Kawano, H., ... Yumoto, K. (2009). Propagation characteristics of pi 2 pulsations observed at high- and low-latitude magdas/cpmn stations: A statistical study. *Journal of Geophysical Research: Space Physics*, *114*(A11). doi: https://doi.org/10.1029/2009JA014163

Uozumi, T., Yoshikawa, A., Ohtani, S., Imajo, S., Baishev, D., Moiseev, A., & Yumoto, K. (2016b). Initial deflection of middle-latitude pi2 pulsations in the premidnight sector: Remote detection of oscillatory upward field-aligned current at substorm onset. *Journal of Geophysical Research: Space Physics*, *121*(7), 6324–6340.

Uozumi, T., Yoshikawa, A., Ohtani, S., Imajo, S., Baishev, D. G., Moiseev, A. V., & Yumoto, K. (2016a). Initial deflection of middle-latitude pi2 pulsations in the premidnight sector: Remote detection of oscillatory upward field-aligned current at substorm onset. *Journal of Geophysical Research: Space Physics*, *121*(7), 6324-6340. doi: https://doi.org/10.1002/2015JA021698

Uozumi, T., Yumoto, K., Kawano, H., Yoshikawa, A., Ohtani, S., Olson, J., ... others (2004). Propagation characteristics of pi 2 magnetic pulsations observed at ground high latitudes. *Journal of Geophysical Research: Space Physics*, *109*(A8).

Uozumi, T., Yumoto, K., Kawano, H., Yoshikawa, A., Olson, J., Solovyev, S., & Vershinin, E. (2000). Characteristics of energy transfer of pi 2 magnetic pulsations: Latitudinal dependence. *Geophysical Research Letters*, *27*(11), 1619–1622.

Uozumi, T., Yumoto, K., Tokunaga, T., Solovyev, S. I., Shevtsov, B. M., Marshall, R., ... Itonaga, M. (2011). Akr modulation and global pi2 oscillation. *Journal of Geophysical Research: Space Physics*, *116*(A6). doi: https://doi.org/10.1029/2010JA016042

Vetterli, M. (1986). Filter banks allowing perfect reconstruction. *Signal processing*, *10*(3), 219–244.

Webster, D. J., Samson, J. C., & Rostoker, G. (1989). Eastward propagation of transient field-aligned currents and pi 2 pulsations at auroral latitudes. *Journal of Geophysical Research: Space Physics*, *94*(A4), 3619-3630. doi: https://doi.org/10.1029/JA094iA04p03619

Xu, Z., Zhu, L., Sojka, J., Kokoszka, P., & Jach, A. (2008). An assessment study of the wavelet-based index of magnetic storm activity (wisa) and its comparison to the dst index. *Journal of Atmospheric and Solar-Terrestrial Physics*, *70*(11), 1579-1588. doi: https://doi.org/10.1016/j.jastp.2008.05.007

yang Zeng, X., & guang Wang, S. (2013). Bark-wavelet analysis and hilbert–huang transform for underwater target recognition. *Defence Technology*, *9*(2), 115-

120. doi: https://doi.org/10.1016/j.dt.2012.09.001

Yeoman, T., & Orr, D. (1989). Phase and spectral power of mid-latitude pi2 pulsations: Evidence for a plasmaspheric cavity resonance. *Planetary and space science*, *37*(11), 1367–1383.

Yumoto, K. (1990). Evidences of magnetospheric cavity pi2 waves. *Journal of geomagnetism and geoelectricity*, *42*(11), 1281–1290.

Yumoto, K., group, C., et al. (2001). Characteristics of pi 2 magnetic pulsations observed at the cpmn stations a review of the step results. *Earth, planets and space*, *53*(10), 981–992.